Journal of Energy Storage 144 (2026) 119680

Contents lists available at ScienceDirect

Journal of Energy Storage

journal homepage: www.elsevier.com/locate/est

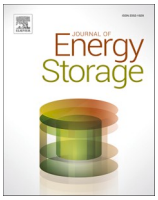

Research Papers

A data-driven and physics-based model for assessing real-world usage behavior impacts on electric vehicle battery life

Hao Jing [a,b], Jianyao Hu [c], Shiqi (Shawn) Ou [a,b,*], Xinwu Qian [d], Hao Qi [a,b], Jiankuan Zhu [a], Haobo Dong [a,b]

[a] School of Future Technology, South China University of Technology, Guangzhou, Guangdong, 511442, China
[b] Guangdong Artificial Intelligence and Digital Economy Laboratory (Guangzhou), Guangzhou, Guangdong 510335, China
[c] China Electronic Product Reliability and Environmental Testing Research Institute, Guangzhou, Guangdong, 510610, China
[d] Department of Civil and Environmental Engineering, Rice University, Houston, TX, United States

ARTICLE INFO

Keywords:
Data-driven
Driver behaviors
Electric vehicles
State of Health
Vehicle-to-Grid

ABSTRACT

Battery life has been well-predicted under controlled laboratory conditions. However, real-world driving and charging behaviors introduce significant variability, making accurate predictions challenging. Factors such as aggressive acceleration, frequent rapid charging, deep discharge cycles, and varying ambient conditions contribute to deviations from laboratory-based degradation models. This study develops the Electric Vehicle-Dynamic Operation Simulation (EV-DOS) model, integrating physics-based and data-driven approaches to address this complexity. The physics-based modules simulate powertrain energy transfer, while a Long Short-Term Memory (LSTM) based data-driven module, trained on real-world vehicle data, enhances accuracy in estimating battery State of Health (SOH) and degradation. The EV-DOS model achieves a monthly average energy consumption error of 0.53 kWh/100 km and a SOH estimation error of 0.6 %, demonstrating high reliability in real-world applications. By applying the validated model across diverse driving conditions, this study identifies key behavioral factors affecting battery degradation, including charging rate, charging depth, ambient temperature, Heating, Ventilation, and Air Conditioning (HVAC) system usage, and Vehicle-to-Grid (V2G) participation. Among these, the charging rate has the most significant impact on SOH deterioration, followed by charging depth and V2G behavior. While higher ambient temperatures can slow SOH degradation by improving battery efficiency, increased HVAC energy consumption under extreme conditions accelerates capacity loss. The EV-DOS model provides actionable insights into optimizing driving and charging behaviors, offering a comprehensive framework for energy management strategies to mitigate battery aging. This research contributes to extending battery lifespan, improving EV reliability, and supporting sustainable transportation by enabling more accurate and personalized battery health predictions.

1. Introduction

To address environmental challenges such as climate change, governments and organizations have implemented policies to promote green transportation, with the Paris Agreement setting carbon reduction targets and the European Commission aiming for a 55 % reduction in greenhouse gas emissions by 2030 [1]. Electric vehicles (EVs), as zero-emission transportation, have become a key pathway to achieving carbon goals [2]. The EV market has rapidly grown over the past decade, reaching a milestone in 2022 when new EV sales exceeded 10 % market share worldwide [3]. By 2024, EV sales are expected to reach 17 million units, accounting for over 20 % of global vehicle sales [4]. Despite their advantages, EV adoption faces challenges, with battery lifespan being a key limitation. The State of Health (SOH) represents battery life and is directly tied to SOH degradation rates [5]. Factors affecting SOH degradation are complex and include production-related aspects and driver behaviors, which significantly impact battery health [6–8]. Therefore, understanding real-world driver behavior effects on battery lifespan and offering optimization recommendations is crucial for both drivers and manufacturers [9]. Many studies, as shown in Table 1, have modeled the impact of different operating factors on battery aging, with Section 1.1 providing a comprehensive overview.

* Corresponding author at: School of Future Technology, South China University of Technology, Guangzhou, Guangdong, 511442, China.
E-mail addresses: sou@scut.edu.cn, oushiqi@pazhou.cn (S.(S. Ou).

https://doi.org/10.1016/j.est.2025.119680
Received 9 February 2025; Received in revised form 18 November 2025; Accepted 30 November 2025
Available online 5 December 2025

Nomenclature

Abbreviations

AKF	Adaptive Kalman Filter
AGU	Adaptive Gradient Update
BP	Back Propagation
BTMS	Battery Thermal Management System
CNN	Convolutional Neural Network
DC FC	Direct Current fast charging
EIS	Electrochemical Impedance Spectroscopy
ELM	Extreme Learning Machine
EKF	Extended Kalman Filter
EV-DOS	Electric Vehicle-Dynamic Operation Simulation
EVs	Electric Vehicles
EC	Energy Consumption
ECM	Equivalent circuit models
GPR	Gaussian Process Regression
GRU	Gated Recurrent Unit
HVAC	Heating, Ventilation, and Air Conditioning
IC	Incremental Capacity
IQR	Interquartile Range
LLS	Linear Least Squares
LSTM	Long Short-Term Memory
MAE	Mean Absolute Error
ME	Maximum Error
MSE	Mean Squared Error
OCV	Open Circuit Voltage
PSO	Particle Swarm Optimization
R^2	Coefficient of Determination
RBS	Regenerative Braking System
RLOESS	Robust Locally Weighted Scatterplot Smoothing
RLS	Recursive Least Squares
RNNs	Recurrent Neural Networks
RMSE	Root Mean Squared Error
RVM	Relevance Vector Machine
SOC	State of Charge
SOH	State of Health
L1	Level 1 Charging
V2G	Vehicle-to-Grid

Variables

F_{pt}	Total tractive force
F_d	Aerodynamic drag
F_r	Rolling resistance
F_g	Grade resistance
F_a	Acceleration resistance
Q_{acc}	Cumulative charge/discharge capacity
N_{deep}	Cumulative deep charge/discharge count
$v_c(t)$	Vehicle speed
θ	Road gradient
W_{pt}	Total driving energy
X_i	Sample point
Z_i	*Z*-score value
σ	The standard deviation of dataset
P_{pt}	Total tractive power
$a_{car}(t)$	Vehicle acceleration
P_{rbs}	Brake energy recovery power
T_{bat}	Battery temperature
T_c	Cabin temperature
T_a	Ambient temperature
P_{bat}	Total battery power
Q_{bat}	Battery pack heat production
Q_{btms}	Heat added to/removed by BTMS
Q_{hvac}	Heat added to/removed by HVAC
P_{hvac}	HVAC energy consumption
I_c	Battery current
P_{btms}	BTMS energy consumption
$C_{bat,r}$	Battery remaining rated capacity
I_{chg}	Charging current
V_{chg}	Charging voltage
E_{chg}	Charging efficiency
$Q(i)$	Single charge/discharge capacity
μ	Mean of the dataset
x_t	Raw input data at time t
h_{t-1}	State at time t-1
f_t	Forget gate
i_t	Input Gate
o_t	Output Gate
C_{t-1}	Memory cell state at time t-1
C_t	Memory cell state at time t
h_t	State at time t
W_f	Forgotten gate weight
b_f	Forgotten gate bias
S_{total}	Cumulative mileage
W_i	Input gate weight
b_i	Input gate bias
W_o	Output gate weight
b_o	Output gate bias
W_c	Cell memory weight
b_c	Cell memory bias
P_{chg}	Charging power
ΔT	Temperature offset
N_{fast_chg}	Accumulated fast charging times

Table 1
Studies on the impact of different operating factors on battery degradation.

Study	Integrated SOH model	Modeling verification	Operational factors analyzed
[21]	Physics-based semi-empirical model using single-cell data	Partial sub-model verification, no overall model validation	Impact of V2G on battery aging
[51]	Physics-based semi-empirical model using single-cell data	No model verification	Impact of V2G on battery aging
[52]	PDE-based physics model using single-cell data	Verified the SOH model only	Impact of charge/discharge rate on battery aging
[53]	Lithium battery aging model based on single-cell data	Verified the aging model only	Impact of DOD on battery aging
[54]	Empirical aging model based on cell data	Verified the aging model only	Impact of storage conditions under different temperatures and SOC on battery aging
Our study	Data-driven aging model based on real-vehicle battery pack data	Verified the model under real driving conditions across different time and space dimensions	Impact of charge rate, charge depth, V2G, and other factors on battery aging under different conditions

1.1. Literature review

Numerous studies have investigated the impact of user behaviors on battery lifespan in real-world scenarios. Xu et al. analyzed the relationship between charging behaviors and battery degradation, identifying charging current as a key factor affecting battery health [10]. Shirk et al. found through a comparative experiment with new Nissan EVs that vehicles using 50 kW Direct Current Fast Charging (DC FC) degraded nearly 4 % faster than those using Level 2 charging after 80,000 km, with the gap widening at higher mileage [11]. Depth of charge and discharge also significantly affect battery SOH, with higher State of Charge (SOC) and Depth of Discharge (DOD) accelerating degradation [12–14]. Operating temperature plays a crucial role [15], with low temperatures being particularly detrimental to battery lifespan [16]. Auxiliary systems, such as the Battery Thermal Management System (BTMS) and Regenerative Braking System (RBS), influence battery longevity, though improper regenerative braking can accelerate aging, especially at high SOC levels [17–19]. Moreover, studies show that the energy consumption of HVAC systems is second only to that of drive motors in EVs. HVAC operation increases overall energy consumption, which accelerates battery degradation and affects its lifespan [20]. While V2G technology can promote grid stability and enhance EV economic value through bi-directional energy flow, some studies indicate that V2G behavior may accelerate battery aging by 9–14 % over a decade [21]. While these studies mainly focus on cell-level experiments, extending them to actual battery packs may introduce deviations. Existing research predominantly examines individual factors, requiring long observation periods and complex processes, making it difficult to draw statistically valid conclusions. Additionally, many studies lack quantitative support, making it challenging to assess the cumulative effects of multiple factors. Therefore, developing a model to quantify these effects with greater precision is essential, reducing experimental costs and facilitating faster evaluations. The core of these models is the battery SOH estimation model. Current SOH estimation methods are broadly categorized into direct measurement, model-based, and data-driven approaches [22,23], as shown in Table 2. Direct measurement methods map SOH to variables like charge and discharge capacity using laboratory data [24,38]. Although simple, this approach overlooks real-world operating conditions, resulting in reduced accuracy over time [39]. Model-based methods include Equivalent Circuit Models (ECM) and electrochemical models. ECMs simulate battery behavior using components like resistors and capacitors, identifying aging-related variables such as temperature and voltage [34,40]. Electrochemical models offer higher accuracy by analyzing internal reactions. However, they are complex, computationally intensive, and have limited practical applications [34,39,41]. These models are often battery-specific, requiring recalibration for different types or conditions [34,42]. Data-driven methods, which are gaining attention with the growth of the Internet of vehicles and big data platforms, utilize large datasets and AI algorithms to establish nonlinear relationships between health features and SOH, offering flexibility and managing uncertainty [42,43]. For instance, Kheirkhah-Rad et al. validated their SOH estimation method using cumulative charge/discharge time from cell data along with Feedforward Neural Networks (FFNN), Support Vector Machines (SVM), and Relevance Vector Machines (RVM) [32]. Similarly, Chen et al. employed an ECM to identify parameters from cell data, improving SOH estimation with a neural network [44]. To overcome the limitations of using a single model, Zhang et al. proposed a convolutional neural network-multi-gate mixture of gated recurrent units (CMMOG) framework for battery SOH estimation [45]. Similarly, Bao et al. introduced a hybrid deep neural network, consisting of a CNN, a variant of LSTM, and a dimension attention mechanism, and validated it across three datasets [46]. To address the challenge of estimating SOH from partial charging segment data, another study integrated an Incremental Energy per SOC (IES) curve with a bidirectional LSTM-reduction model, which significantly improved the generalization ability and robustness of SOH estimation [47].

However, Most of these approaches rely on battery cell data obtained under controlled laboratory conditions with predefined loads and temperatures, whereas real-world EV operating environments are much more complex [48]. Additionally, using only cell data to assess battery pack performance presents limitations, as a pack consists of multiple cells with potential manufacturing variations. Real-world battery pack performance is influenced by factors such as thermal management, energy scheduling, and system collaboration, which are difficult to replicate fully in laboratories [48,49]. To improve battery lifespan predictions, it's crucial to model battery pack performance based on real-world data under diverse conditions. Hong et al. utilized real-world data and a Gated Recurrent Unit (GRU) network to model SOH with an error of less than 4 % [33]. Zhao et al. utilized stable charging segments from real-world data, achieving an SOH estimation error of less than 0.5 % with an Extreme Learning Machine (ELM) network [34]. Yi Soo et al. used electric bus data, incorporating ambient temperature, and achieved a mean absolute error (MAE) of less than 0.05 [50]. These studies validate the potential of using real-world data for SOH modeling. However, relying solely on SOH models is insufficient to capture the impact of diverse driving behaviors. Driver operation factors and operating condition data are often not directly usable as inputs to the SOH model. To address this, numerous studies have combined SOH models with physically based energy transfer models for EV powertrains. Physical energy transfer models simulate operational variables such as battery current, voltage, and temperature based on real-world conditions—including vehicle speed, road gradient, and ambient temperature—and convert these variables into inputs suitable for the SOH model. For instance, some studies combined SOH models with EV energy models to examine the impact of V2G on battery aging [21,51]. Bashash et al. studied charge/discharge rates on battery aging using a battery lifetime model combined with a PHEV powertrain model [52]. Millner

Table 2
Classification of SOH estimation methods.

Classification	Specific type	Method	Accuracy	Complexity	Generalizability
Measurement		Coulomb counting [24]	★★☆☆☆	★★☆☆☆	★★★☆☆
		OCV [25]	★★☆☆☆	★★☆☆☆	★★★☆☆
Model-based		EIS [26]	★★★★☆	★★★★★	★★★★☆
		EKF [27]	★★★☆☆	★★★☆☆	★★★☆☆
	ECM	AKF [28]			
		Fractional order-RLS [29]			
	Electrochemical	LLS-AGU [30]	★★★★☆	★★★★★	★★★★☆
		Single particle model [31]			
Data-driven		RVM [32]	★★★★☆	★★★☆☆	★★★★☆
		GRU [33]			
		PSO-ELM [34]			
		CNN-LSTM [35]			
		SSA-GRU [36]			
		CNN-EFC-BiLSTM [37]			

et al. integrated degradation models with equivalent circuit models to analyze the effects of temperature and depth of discharge [53]. However, these studies mainly validate the SOH models without verifying the entire model, leaving their accuracy in question. Additionally, they generally focus on the impact of individual factors on battery degradation.

1.2. Existing challenges in estimating behavioral impacts on SOH

Although a large number of studies have modeled the impact of different operating factors on battery aging, several challenges remain:

1) Purely physical models are complex and computationally intensive, while purely data-driven models make it difficult to quantify the impact of operating factors directly on battery aging. Additionally, most existing SOH models are based on laboratory cell data, which cannot accurately reflect the actual degradation of real-world vehicles.
2) Most existing models lack validation across diverse spatiotemporal dimensions and complex operating conditions, which compromises their applicability and accuracy under different environmental and operational conditions.
3) Most studies have only analyzed the impact of single-driver operation factors on battery aging.

1.3. Study contributions

To address the challenges mentioned above, this study proposes the EV-DOS model, which integrates data-driven and physics-based approaches to predict the long-term impacts on battery health. Leveraging

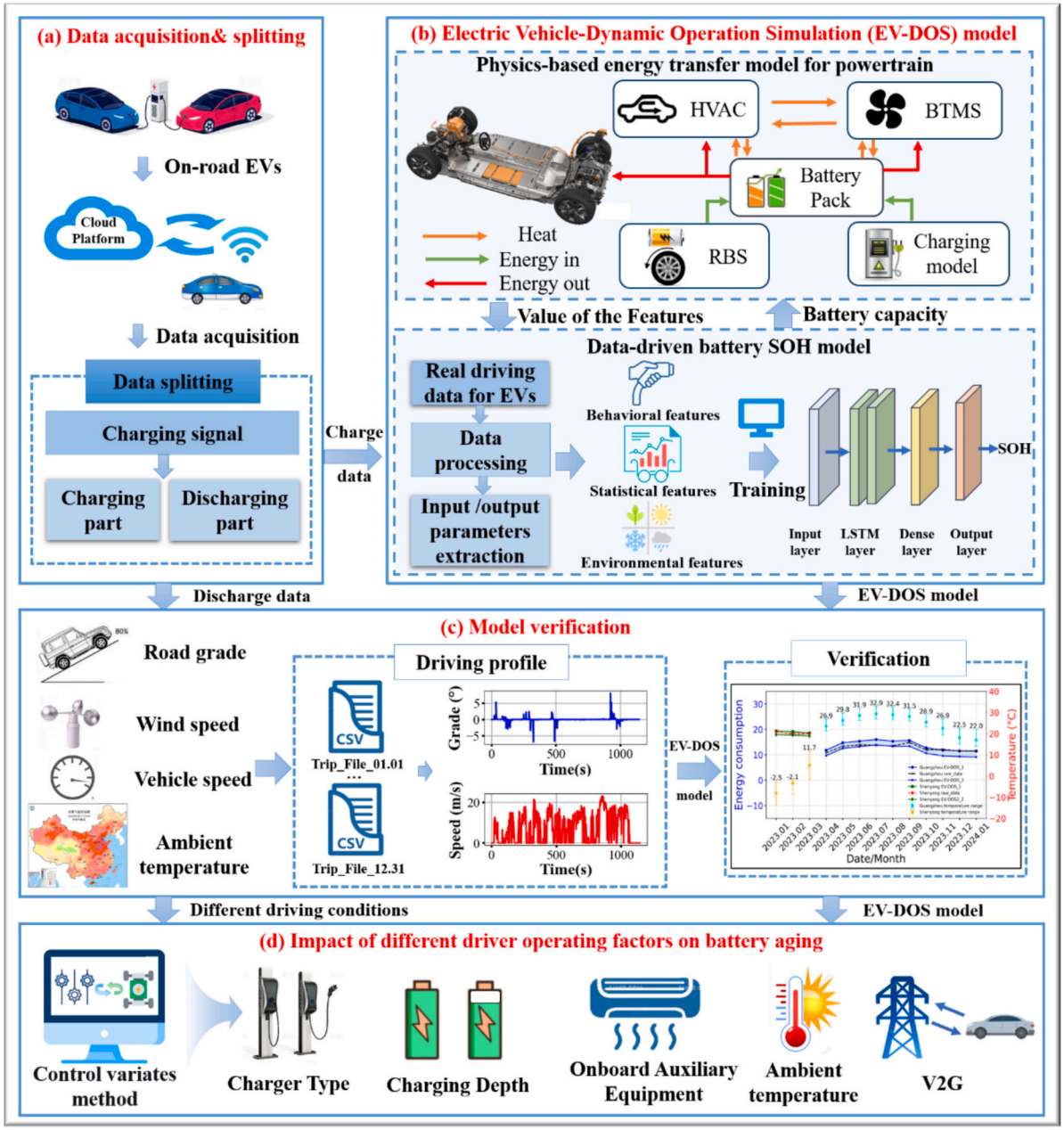

Fig. 1. The logic diagram of the research. (a) Real-world vehicle data acquisition and partitioning. (b) Construction of the EV-DOS model: The complete simulation framework is constructed by bidirectionally coupling the physics-based powertrain energy transfer model with the data-driven SOH model based on real-world vehicle operation data. (c) Model verification using real driving data. (d) Impact of operating factors on battery aging under different driving conditions.

real-world driving data, the model extracts critical aging-related health parameters inaccessible in laboratory environments and develops a high-precision SOH estimator using an LSTM neural network. The framework bridges the gap between physical vehicle dynamics and data-driven SOH prediction by coupling the LSTM model with physics-based sub-models encompassing vehicle dynamics, charging protocols, and V2G interactions. This hybrid architecture quantifies the correlations between SOH degradation and operational variables, enabling the scalable analysis of driving behavior's impact on battery lifespan. Comprehensive validation demonstrates robust alignment of energy consumption and degradation patterns across diverse driving scenarios, spatiotemporal scales, and temporal resolutions. Furthermore, the study identifies key behavioral factors influencing battery degradation. It evaluates their cumulative aging effects through longitudinal EV-DOS simulations, establishing a systematic framework for optimizing EV battery management under dynamic operational conditions.

1.4. Organization of the paper

This paper is organized into six sections: The first section explains the motivation for the research and provides the relevant background. The second section details the construction of the EV-DOS model. The third section describes the data used and the processing steps. The fourth section presents the simulation results and validation of the EV-DOS model. The fifth section quantifies the effects of different driving behaviors on battery SOH and provides practical recommendations. The final section summarizes the research findings and outlines directions for future work.

2. Method

To accurately evaluate battery lifetime under different road conditions and driving scenarios, this study develops a high-fidelity EV-DOS model. As shown in Fig. 1, in contrast to previous studies that rely solely on physics-based modeling or purely data-driven approaches, the EV-DOS model bidirectionally couples a physics-based powertrain energy-transfer model with a battery SOH estimation module constructed from real-world vehicle operation data, thereby overcoming the limitations of traditional single-paradigm modeling approaches. Specifically, the physics-based EV powertrain model integrates vehicle dynamics, thermodynamics, and V2G interaction modules to compute key quantities such as energy consumption, current, voltage, and temperature during vehicle operation. In this way, it accurately simulates the processes of energy transfer and conversion under diverse driving and environmental conditions, while ensuring physical interpretability and adherence to physical constraints. On the data-driven side, the SOH model leverages real-world operational data to construct a feature space that incorporates multiple categories of driving behaviors and environmental factors, and employs an LSTM neural network to estimate the battery health state. This enables the simulation and quantification of the complex nonlinear relationships between battery aging and various driving behaviors and environmental conditions. Such complex dependencies arising from real-world operating scenarios are difficult to capture effectively using conventional models based on single-cell data measured under controlled conditions. During simulation, the battery current, temperature, and other parameters output by the physics-based model are passed as inputs to the trained LSTM model, which is then used to update the SOH of the battery pack. The updated SOH information is subsequently fed back into the physics-based model, forming a dynamic interaction between the two modules. Through the organic integration of these components, a comprehensive battery lifetime simulation framework is established that effectively combines the rigor of physics-based mechanisms with the flexibility of data-driven modeling. This closed-loop simulation structure enables scalable, robust, and personalized battery lifetime prediction across various driving and charging scenarios.

2.1. Physics-based energy transfer model for powertrain

2.1.1. Powertrain power calculation module

The powertrain is modeled using a backward modeling approach. First, based on longitudinal vehicle dynamics and input conditions such as vehicle speed and road gradient, the total tractive force required for vehicle movement is calculated [55], as presented in Eqs. (1)–(5):

$$F_{pt} = F_d + F_r + F_g + F_a \tag{1}$$

$$F_d(t) = \frac{1}{2}\rho_{air} A_d c_d (v_c(t) - v_{\text{wind}})^2 \tag{2}$$

$$F_r(t) = c_r m_v g \cos(\theta) \tag{3}$$

$$F_g(t) = m_v g \sin(\theta) \tag{4}$$

$$F_a(t) = \sigma m_v a_{car}(t) \tag{5}$$

where F_{pt} is the total tractive force required for vehicle operation, F_d is the aerodynamic drag, F_r is the rolling resistance, F_g is the grade resistance, F_a is the acceleration resistance, $v_c(t)$ denotes the vehicle speed, and θ represents the road gradient.

Based on the total tractive force calculated from the above equation, the driving power required for vehicle movement can be calculated through Eq. (6):

$$P_{pt} = \frac{dW_{pt}}{dt} = F_{pt} v_c(t) \tag{6}$$

where W_{pt} is the driving energy required for vehicle movement.

During braking, part of the energy is recovered by the RBS and stored in the battery by reversing the motor. In this study, it is assumed that energy is recovered to the battery at a constant efficiency during braking and can be calculated through Eq. (7):

$$P_{rbs} = P_{pt} \bullet f_{rbs} \tag{7}$$

where P_{rbs} is the power for energy recovery during braking, f_{rbs} is the efficiency of braking energy recovery.

2.1.2. Heat transfer module

Temperature is a crucial factor affecting battery aging, and therefore, it is necessary to incorporate the modeling of battery temperature into the vehicle dynamics model. As shown in Fig. 1, this study examines the heat exchange between the battery and the vehicle cabin, modeling both the BTMS and the HVAC systems of the EV. During operation, the battery temperature is calculated using Eqs. (8)–(10):

$$C_{bat}\frac{dT_{bat}}{dt} = K_{ab}(T_a - T_{bat}) + K_{bc}(T_c - T_{bat}) + \frac{dQ_{btms}}{dt} + \frac{dQ_{bat}}{dt} \tag{8}$$

$$P_{btms} = \frac{dQ_{btms}}{dt} = -K_{btms} \bullet \min\left(T_{bat} - T_{b,up}, 10\right), \text{where } T_{bat} \geq T_{b,up} \tag{9}$$

$$P_{btms} = \frac{dQ_{btms}}{dt} = K_{btms} \cdot \min\left(T_{b,\text{low}} - T_{bat}, 10\right), \text{where } T_{bat} \leq T_{b,\text{low}} \tag{10}$$

where T_{bat} is the battery temperature, T_c is the cabin temperature, T_a is the ambient temperature,Q_{btms} is the heat dissipation/heating energy for the operation of the BTMS, Q_{bat} is the heat emitted by the battery pack when it is in operation [55].

The cabin temperature is calculated through Eqs. (11)–(13):

$$C_c\frac{dT_c}{dt} = K_{ac}(T_a - T_c) + K_{bc}(T_{bat} - T_c) + \frac{dQ_{hvac}}{dt} \tag{11}$$

$$\begin{cases} \dfrac{dQ_{hvac}}{dt} = 4, & T_c < 18.85^{\circ}C \\ \dfrac{dQ_{hvac}}{dt} = -1.7\cdot(T_c + 273.15) + C_{HVAC}, & 18.85^{\circ}C \le T_c \le 23.88^{\circ}C \\ \dfrac{dQ_{hvac}}{dt} = -4.5, & T_c > 23.88^{\circ}C \end{cases} \quad (12)$$

$$\begin{cases} P_{hvac} = \dfrac{|Q_{hvac}|}{COP_{cooling}}, HVAC\ \text{cooling}, Q_{hvac} < 0 \\ P_{hvac} = \dfrac{|Q_{hvac}|}{COP_{heating}}, HVAC\ \text{heating}, Q_{hvac} \ge 0 \end{cases} \quad (13)$$

where Q_{hvac} is the heat added to or removed from the cabin by the vehicle's HVAC system, P_{hvac} is the power consumed for HVAC systems [55].

2.1.3. Battery state estimation and power calculation module

As shown in Fig. 1, the battery provides energy for vehicle propulsion, HVAC operation, and BTMS. The RBS also recovers part of the energy and returns it to the battery. Therefore, during vehicle operation, the total power input/output of the battery pack can be expressed by Eq. (14):

$$P_{bat} = P_{pt} + P_{hvac} + P_{btms} + P_{rbs} \quad (14)$$

where P_{bat} is the total power of the battery.

The relationship between the current and power of an electric vehicle while driving is calculated through Eq. (15):

$$P_{bat} = (OCV + I_c \bullet R_{bat}) \bullet I_c \quad (15)$$

where OCV is the open circuit voltage of the battery pack, R_{bat} is the internal resistance of the battery pack, I_c is the battery pack input/output current.

The battery SOC is updated using the coulomb-counting equation, as given in Eq. (16):

$$SOC = SOC_0 - \frac{\int I_c dt}{C_{bat,r}} \quad (16)$$

where SOC_0 is the initial SOC, and $C_{bat,r}$ is the remaining rated capacity of the battery pack. The main parameters of vehicle powertrain modeling are shown in Appendix Table A.1.

2.1.4. Charging module

When the daily journey is completed, or the battery SOC falls below 1 %, the model initiates a charging process. During charging, the current direction is opposite to that of discharging during vehicle operation, leading to an increase in SOC. Charging stops either when the charging duration reaches the available charging time or when the SOC reaches the target level. The charging current is represented through Eq. (17):

$$I_{chg} = P_{chg}\cdot E_{chg} / V_{chg} \quad (17)$$

where I_{chg} is the charging current, E_{chg} is the charging efficiency, and V_{chg} is the charging voltage.

2.1.5. V2G discharging module

The V2G model established in this study aims to simulate the battery discharging to the grid through the charging pile. During discharging, it is assumed that the EV outputs a constant current, as represented by Eq. (18):

$$I_{dischg} = P_{dischg}\cdot E_{dischg} / V_{dischg} \quad (18)$$

where I_{dischg}, E_{chg}, V_{chg} are the discharging current, discharging efficiency, and the discharging voltage during V2G, respectively.

2.2. Data-driven battery SOH model

Battery SOH evolution is a gradual process influenced by time-dependent factors such as historical charging/discharging behavior and environmental conditions, which exhibit significant temporal dependencies. Consequently, Recurrent Neural Networks (RNNs), effective for time series data, have gained research attention [42,56]. RNNs excel at capturing dynamic features and temporal dependencies, but traditional RNNs struggle with vanishing or exploding gradients when modeling long-term sequences. To address this, LSTM and GRU networks were developed, with LSTM offering superior long-term dependency modeling due to its independent cell state and sophisticated gating mechanisms, making it ideal for tasks like battery SOH prediction. As shown in Fig. 2, the LSTM cell uses three gates to control the information flow at each time step t. Given the current input x_t and the previous hidden state h_{t-1}, the forget gate f_t, input gate i_t, and output gate o_t are computed as in Eqs. (19)–(21):

$$f_t = \sigma\left(W_f\cdot[h_{t-1}, x_t] + b_f\right) \quad (19)$$

$$i_t = \sigma(W_i\cdot[h_{t-1}, x_t] + b_i) \quad (20)$$

$$o_t = \sigma(W_o\cdot[h_{t-1}, x_t] + b_o) \quad (21)$$

The cell state C_t and hidden state h_t are then updated according to Eqs. (22)–(23):

$$C_t = f_t \odot C_{t-1} + i_t \odot \tanh(W_c\cdot[h_{t-1}, x_t] + b_c) \quad (22)$$

$$h_t = o_t \odot \tanh(C_t) \quad (23)$$

where, W_f, b_f, W_i, b_i, W_o, b_o, W_c and b_c represent the weight matrices and bias terms, respectively.

Furthermore, in contrast to conventional SOH modeling approaches that rely solely on cell-level data, the LSTM model developed in this study substantially expands the input feature space. As illustrated in Fig. 1(b), the input features are systematically constructed and categorized into three groups: real-world driver behavioral features, statistical features, and environmental conditions, thereby capturing the key factors that govern battery aging under practical vehicle usage. The detailed feature engineering procedures are presented in Section 3.2.1.

3. Data used

3.1. Data acquisition and preprocessing

3.1.1. Data acquisition

This study utilizes real-world operational data from ride-hailing passenger vehicles over 12 months to capture their operating conditions and assess their health status. The dataset, comprising over two million records, provides a comprehensive view of vehicle behavior under actual driving scenarios. Fig. 3 presents the raw operational data of a specific vehicle, with key parameters listed in Table 3. Fig. 3(a) displays the recorded signals, including vehicle speed, charging status, total current, and voltage, for dynamic monitoring purposes. Based on these signals, the time distribution across driving, charging, and idle states is obtained, as illustrated in Fig. 3(b). Fig. 3(c) further presents a two-month activity heatmap, indicating that the vehicle primarily operates in Guangzhou's Panyu district, thereby revealing typical driving patterns and road conditions.

3.1.2. Data preprocessing

External factors such as road conditions, traffic, and weather introduce noise and inconsistencies in onboard sensor data. Signal fluctuations during transmission further compromise data integrity, resulting in duplicates, outliers, and missing values. The use of unprocessed data would significantly degrade the accuracy of SOH estimation,

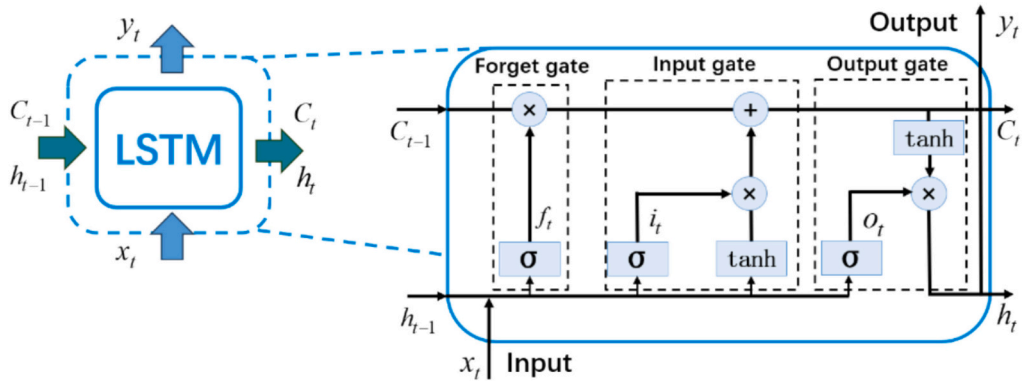

Fig. 2. LSTM neural network architecture.

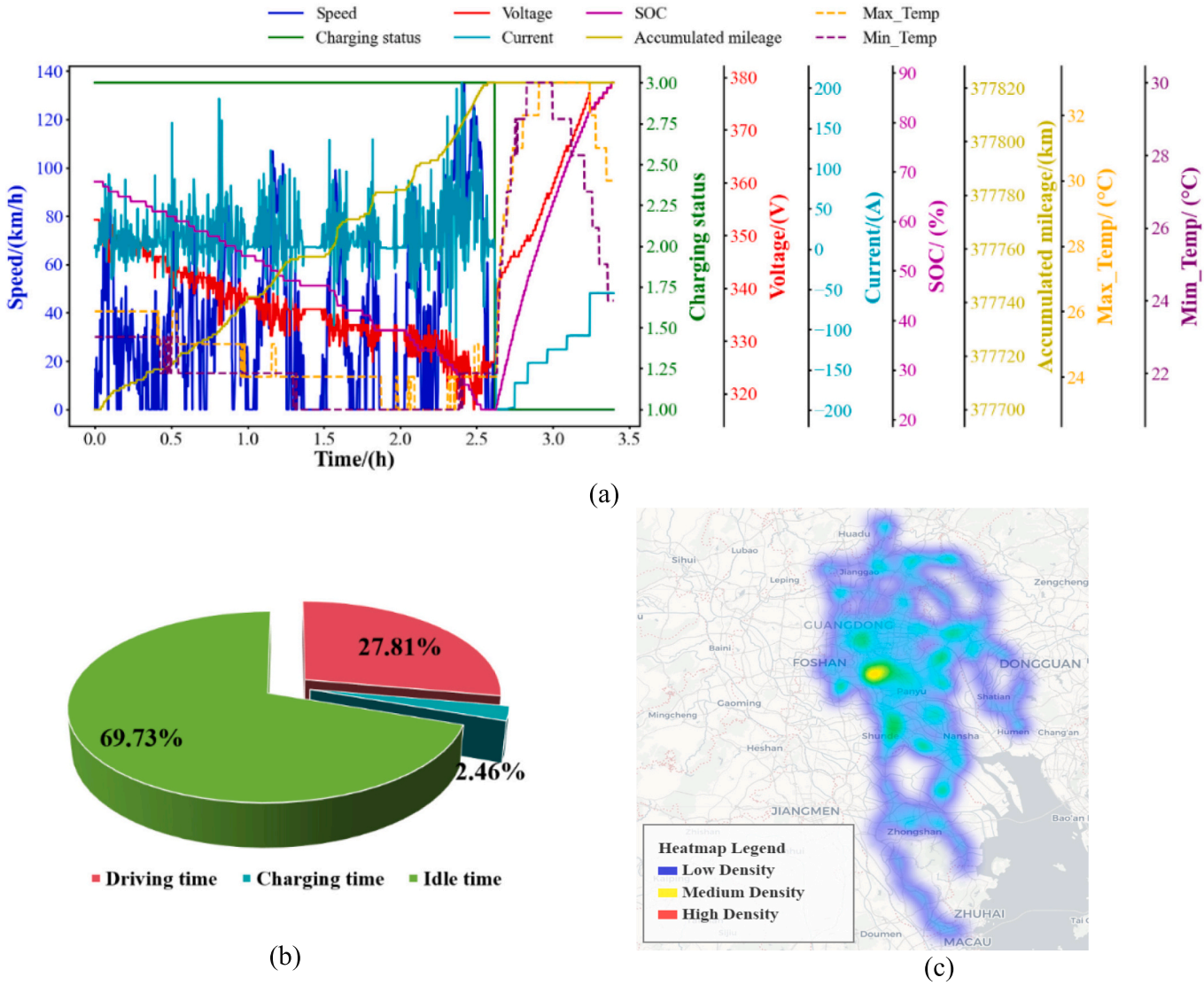

Fig. 3. Real-world vehicle collection raw data. (a) Vehicle single charge-discharge raw data graph. (b) The percentage contribution of charging, driving, and idle time in the collection of data. (c) Two-month vehicle activity heatmap.

underscoring the necessity for rigorous preprocessing, as highlighted in prior studies [34,57].

The preprocessing workflow, illustrated in Fig. 4, begins with the removal of duplicate entries based on timestamps to ensure the uniqueness of the time-series data. Given the absence of environmental temperature records in the dataset, historical weather data from Visual Crossing Weather [58] was integrated to enhance the reliability of the analysis. Subsequently, outlier detection was performed using the

Table 3
Collected vehicle-related parameters and characteristics.

Parameters	Value	Parameters	Value
Vehicle speed range	0–140 km/h	Vehicle weight	1650 kg
Total voltage range	310–400 V	Battery pack energy	64 kWh
Total current range	−200-320 A	Total motor power	100 kW
Cell number	91	Cell voltage range	3.4–4.3 V
Battery capacity	150 Ah	Battery temperature range	18–47 °C

Interquartile Range (IQR) method, which identifies values that fall beyond 1.5 times the IQR [59]. This process is visually represented in Fig. 5(a). Following outlier detection, the data were segmented into distinct charging and discharging periods. However, this segmentation revealed gaps and missing values, as depicted in Fig. 5(b). To address this, interpolation techniques were employed to complete the time series, thereby ensuring data continuity.

Additionally, since the dataset lacked road gradient information, elevation data were retrieved using Open Topo Data [60] based on the latitude and longitude coordinates. Fig. 6 provides a visual representation of vehicle activity areas and elevation changes over two months, revealing an elevation range of within 10 m. Utilizing this elevation and displacement data, road gradients were calculated according to Eq. (24):

$$\theta = \arctan\left(\frac{\Delta h}{\Delta d}\right) \tag{24}$$

where Δh is the amount of elevation change, Δd is the displacement.

3.2. Health features extraction and capacity label calculation

3.2.1. Battery health features extraction

The accuracy of data-driven LSTM models heavily depends on feature selection, making feature extraction critical for battery SOH. Variations in data types across vehicles and the inclusion of all potential health features can increase model complexity, introduce redundancy, and impact generalizability [33,34]. Therefore, identifying a set of relevant and broadly applicable health features is essential.

As battery cycle counts rise, irreversible changes in electrode materials lead to performance degradation. Real-world usage rarely involves complete discharge and recharge cycles, so cumulative mileage and cumulative charge/discharge capacity were selected as key features due to their strong correlation with cycle counts. Cumulative mileage indicates battery workload, while cumulative capacity reflects total energy throughput, capturing degradation aspects [34,61].

Battery health is also affected by current intensity and charging methods. Excessive current and fast charging generate heat, accelerating degradation and potentially causing lithium dendrite formation, which can lead to internal short circuits. To address this, the study included average current, average charging power, and the cumulative number of fast charging events, where charging sessions exceed 35 kW, as health features [62].

Deep charge/discharge cycles stress electrode materials and intensify degradation, especially under extreme SOC. This study defined deep discharge as SOC below 15 % and deep charge as SOC above 95 %, incorporating their cumulative counts as critical features [13,34].

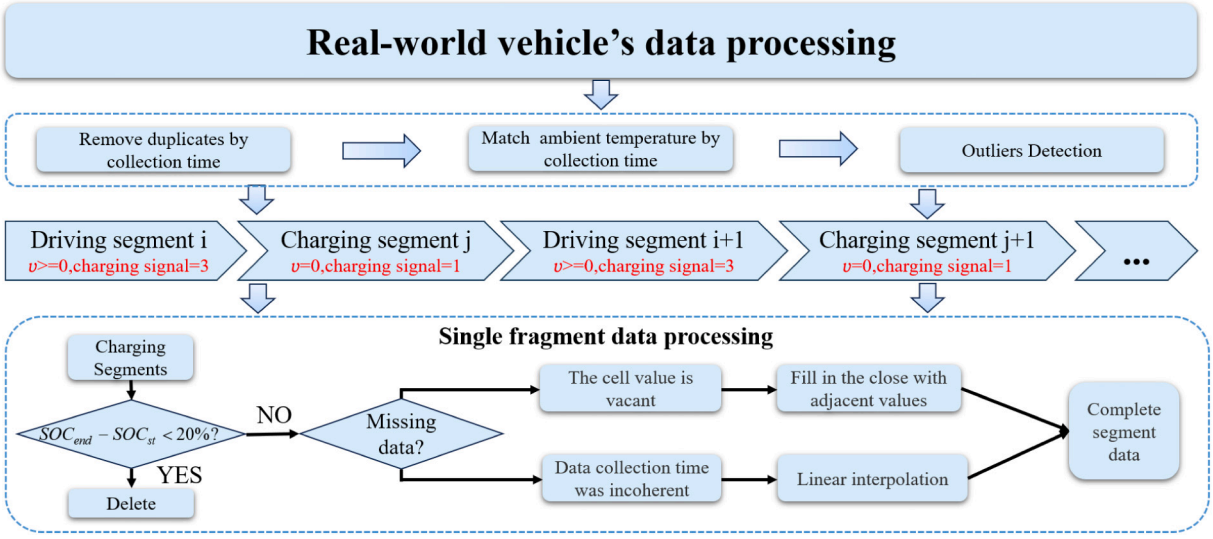

Fig. 4. Real-world vehicle data pre-processing flow chart.

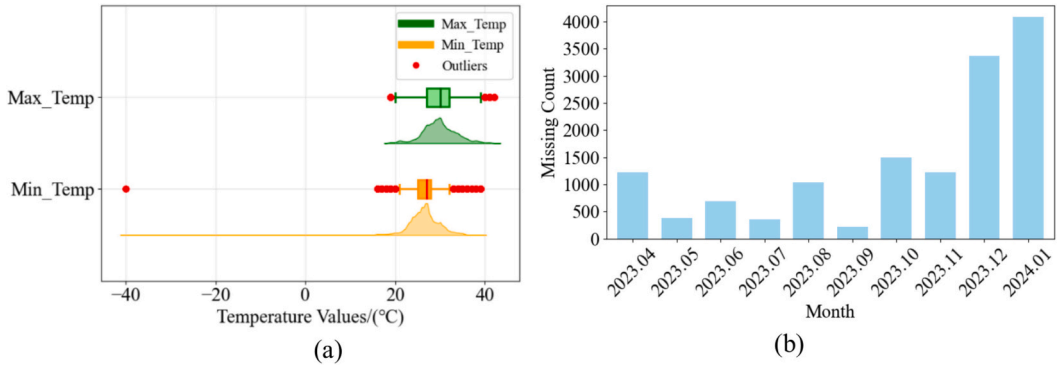

Fig. 5. Real-world vehicle data information. (a) Distribution chart of maximum and minimum temperature values. (b) Data missing distribution chart.

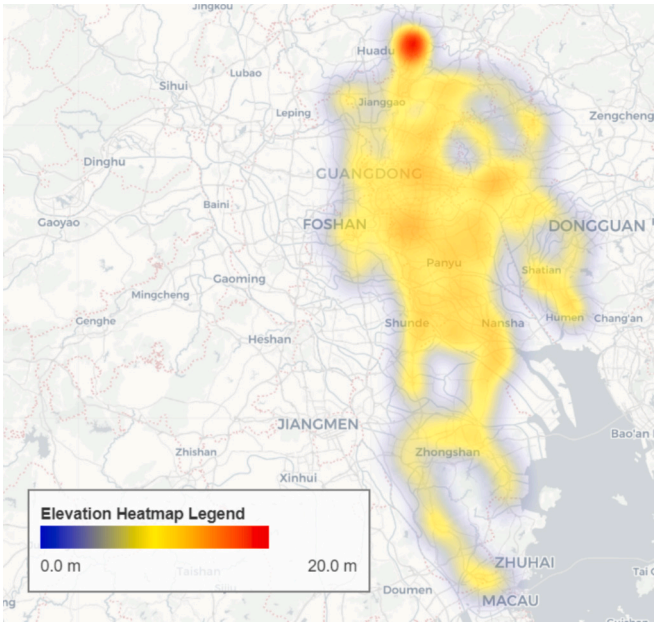

Fig. 6. The two-month activity area and location elevation heatmap of an example vehicle.

Temperature plays a significant role in determining battery performance and lifespan, with optimal operation occurring between 20 °C and 25 °C. High temperatures accelerate material decomposition, while low temperatures increase resistance. This study included deviations from a 25 °C baseline in average battery temperature, along with ambient temperature, to capture both internal and external environmental impacts [16,63].

3.2.2. *Reference capacity and SOH calculation*

The SOH of a battery is typically measured by internal resistance or remaining capacity [33,34,48]. However, due to the significant impact of external factors like ambient temperature on internal resistance, this study uses the remaining maximum available capacity as the SOH indicator. As shown in Fig. 3(a), current fluctuations during discharging, caused by real-world conditions such as acceleration, deceleration, and climbing, are substantial. Additionally, limitations in sampling frequency and sensor accuracy introduce errors in calculating the remaining capacity during discharging, making it difficult to accurately reflect the battery's actual state. In contrast, during charging, the current exhibits a more stable, stepwise, constant characteristic. Therefore, this study uses each charging segment as an analysis window, calculating the remaining maximum capacity to better represent SOH. The calculation formula based on charging phase data is given in Eq. (25) [34,64]. The specific calculation method is shown in Eq. (25):

$$C_{bat,r} = \frac{Q(i)}{\Delta SOC} = \frac{\int_{t_0}^{t_1} I(t)dt}{SOC(t_1) - SOC(t_0)} \tag{25}$$

where $Q(i)$ is the single charge capacity, $I(t)$ is the real-time current, $SOC(t_1)$ is the SOC at the end of the charging segment, and $SOC(t_0)$ is the SOC at the beginning of the charging segment. The distributions of $SOC(t_1)$ and $SOC(t_0)$ are shown in Fig. 7(a) and (b). ΔSOC represents the change in SOC for the charging segment. A smaller ΔSOC will lead to greater calculation errors and fluctuations, whereas a larger ΔSOC typically results in too few usable charging segments, leading to insufficient training data and preventing the model from fully learning the information [34,50,64]. As shown in Fig. 4, this study selects only segments with a greater than 20 % increase, and the distribution is presented in Fig. 7(c).

The battery health state is calculated as shown in Eq. (26):

$$SOH = \frac{C_{bat,r}}{C_{rated}} \tag{26}$$

where C_{rated} is the factory capacity of the battery.

Through the calculation of the vehicle data, a total of 347 SOH values from charging segments were obtained, as shown in Fig. 7(d). Because sensor errors and communication noise introduce spikes and discontinuities that hinder model training, the SOH series is first cleaned using a Z-score-based outlier filter [34]. After outlier removal, a Robust Locally

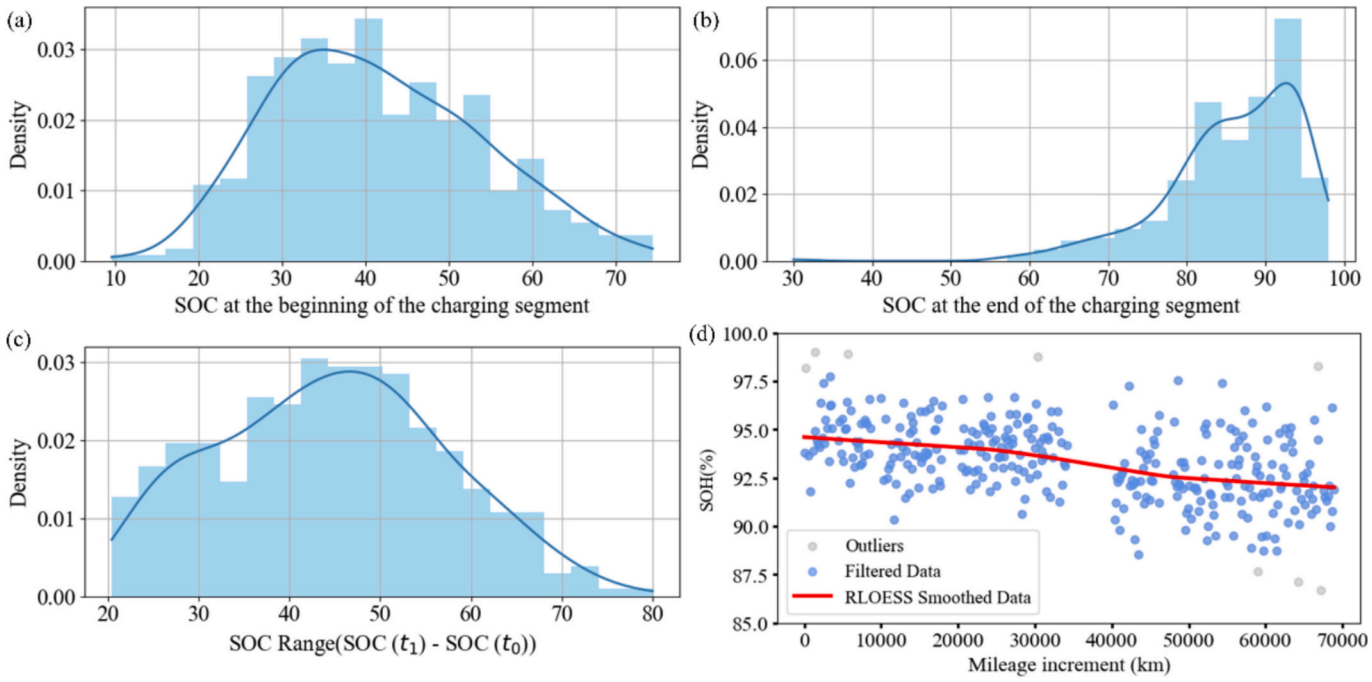

Fig. 7. Distribution of SOC in charging segments and calculated reference SOH. (a) Distribution of SOC at the beginning of the charging segment. (b) Distribution of SOC at the end of the charging segment. (c) Distribution of the SOC variation range. (d) Calculated reference SOH.

Weighted Scatterplot Smoothing (RLOESS) filter is applied to reduce fluctuations further and enhance the continuity of the SOH data. RLOESS, a non-parametric smoothing method based on locally weighted regression, suppresses random noise while preserving the curve's overall trend, making it ideal for nonlinear and noisy data [34,65]. As shown in Fig. 7(d), the smoothed SOH curve exhibits a smoother trend with significantly reduced fluctuations compared to the original data.

4. Modeling results

4.1. The LSTM-based SOH model training and comparison

Based on the previously extracted real-world vehicle features and reference SOH, this study determined the model inputs, outputs, and neural network types to be used. This study constructed RNN, GRU, and LSTM models to estimate battery SOH and performed a comparative analysis. The LSTM model's hyperparameters are summarized in Table 4. The dataset was divided chronologically, with the first 80 % used for training and the remaining 20 % for testing, to prevent information leakage from future data and ensure temporal consistency and generalization in model evaluation [42]. Fig. 8 presents the SOH estimation results and error profiles for each model during both training and testing. The LSTM model's estimated SOH is closest to the reference data, with minimal fluctuation, showing higher stability and accuracy. Additionally, the LSTM model's estimation error is significantly lower than that of the RNN and GRU models, highlighting its superior ability to handle complex temporal features. To further quantify model performance, a comparative analysis was conducted during the testing phase using several metrics, including Maximum Error (ME), Coefficient of Determination (R^2), Mean Squared Error (MSE), Mean Absolute Error (MAE), and Root Mean Squared Error (RMSE). The results, shown in Fig. 9, indicate that all models have maximum estimation errors of less than 0.1 %. However, in terms of MSE, MAE, and RMSE, the LSTM model outperformed the RNN and GRU models, demonstrating lower errors and higher precision. Consequently, the LSTM model was selected for integration with the physical energy transfer model to form the EV-DOS model for joint simulation.

4.2. The EV-DOS model simulation and calibration

The trained LSTM SOH model, integrated with the physics-based energy transfer model, forms the EV-DOS model. This study conducted simulations and validations of the EV-DOS model under various operating conditions and environmental scenarios. The model requires input parameters, including vehicle speed, road gradient, wind speed, and ambient temperature. Real operational data from multiple ride-hailing vehicles, collected in section 3.1, were used to ensure accuracy and replicate actual driving behavior. Data segments corresponding to the vehicle's motion state, indicated by a charging status signal value of 3, were selected as input. A complete driving and charging cycle is defined as a single driving profile. Fig. 10 presents the input data for a specific day, where the Status field indicates the vehicle's mode: “RunOn” signifies driving mode and “RunOff” indicates charging mode.

As illustrated in Fig. 11, the operational flowchart of the EV-DOS model is presented. After configuring the driving document, the model can be simulated. The EV-DOS model developed in this study is implemented in Python, allowing users to customize various settings before simulation, including defining the cumulative simulation years and adjusting vehicle parameters. Once the simulation begins, the physics-driven powertrain energy module calculates key parameters, such as real-time battery power and temperature, based on information from the driving document, including vehicle speed and road gradient. When a day's driving task is completed, or the battery's SOC falls below 1 %, the system switches to charging mode. The charging phase ends when the battery reaches the target SOC or when the maximum allowable charging time is reached. Subsequently, the accumulated mileage, cumulative charge/discharge capacity, battery temperature deviation, and other features calculated during the simulation are fed into the trained LSTM-based SOH model to update the battery's latest SOH status. Through this iterative process, the model sequentially completes the simulation tasks for each driving profile.

Table 4
Hyperparameters of the LSTM neural network.

Parameters	Description	Value
Epochs	Training iterations	50
Batch size	Minibatch capacity	16
Number of neurons (first layer)	Units in the first LSTM layer.	64
Number of neurons (second layer)	Units in the second LSTM layer	16
Initial learning rate	Starting optimization step size	0.01

To validate the accuracy and generalizability of the model, this study considered both spatial and temporal characteristics, randomly selecting two vehicles from Guangzhou, China, two from Shenyang, China, and one from Tianjin, China, for analysis. The temperature range in the operational environment of these vehicles varied from −15 °C to 33 °C, encompassing significant regional differences and seasonal variations, thereby reflecting diverse climate conditions. This design provides robust support for assessing the model's adaptability and robustness in a wide range of real-world application scenarios. First, since the EV-DOS model aims to simulate the real energy transfer behavior of vehicles, it is essential to validate energy consumption during vehicle operation. Fig. 12(a) and (b) presents the comparison between the actual monthly average energy consumption of the five vehicles and the energy consumption simulated by the EV-DOS model. In these figures, the line plots and shaded areas represent the energy consumption data of the vehicles. At the same time, the error bars provide temperature-related information: the lowest point indicates the monthly average minimum temperature, and the middle point represents the monthly average temperature. The highest point corresponds to the monthly average maximum temperature.

It is well known that vehicle mass has a significant impact on energy consumption. Since the data used in this study comes from ride-hailing passenger vehicles, the vehicle mass fluctuates depending on the number of passengers. An average passenger weight of 70 kg was assumed, with a maximum passenger capacity of four people per vehicle, excluding the driver. Based on this, the total vehicle mass was assumed to vary within the range of 0 to 280 kg. Additionally, due to limitations in wind data and the difficulty of precisely determining tailwind or headwind conditions during vehicle operation, this study assumed a wind speed range of −1.5 m/s to 1.5 m/s. On this basis, in Fig. 12(a) and (b), the upper limit of the simulated energy consumption range corresponds to conditions with full load and headwind. In contrast, the lower limit represents conditions with no load and tailwind.

As shown in Fig. 12(a) and (b), the monthly average energy consumption per 100 km for the five vehicles ranges between 10 and 21 kWh/100 km. Despite variations in driving environments and behaviors among different drivers, the energy consumption simulated by the EV-DOS model aligns closely with the actual data, with a maximum absolute error of only 0.53 kWh/100 km. Further analysis of Fig. 12 reveals that vehicle energy consumption increases significantly under extremely high or low temperatures. This is primarily due to the increased power demand of the HVAC system and the BTMS. Under extreme temperature conditions, whether in intense heat or severe cold, the energy consumption of these auxiliary systems increases significantly, resulting in a rise in overall energy consumption. This result aligns well with real-world driving experiences, fully validating the accuracy of the EV-DOS model in simulating energy consumption under complex environmental conditions. The validation results of this study indicate that the EV-DOS model exhibits strong robustness and consistency in coping with environmental variations. It can accurately simulate the energy transfer and consumption patterns of the vehicle, even under dynamic driving

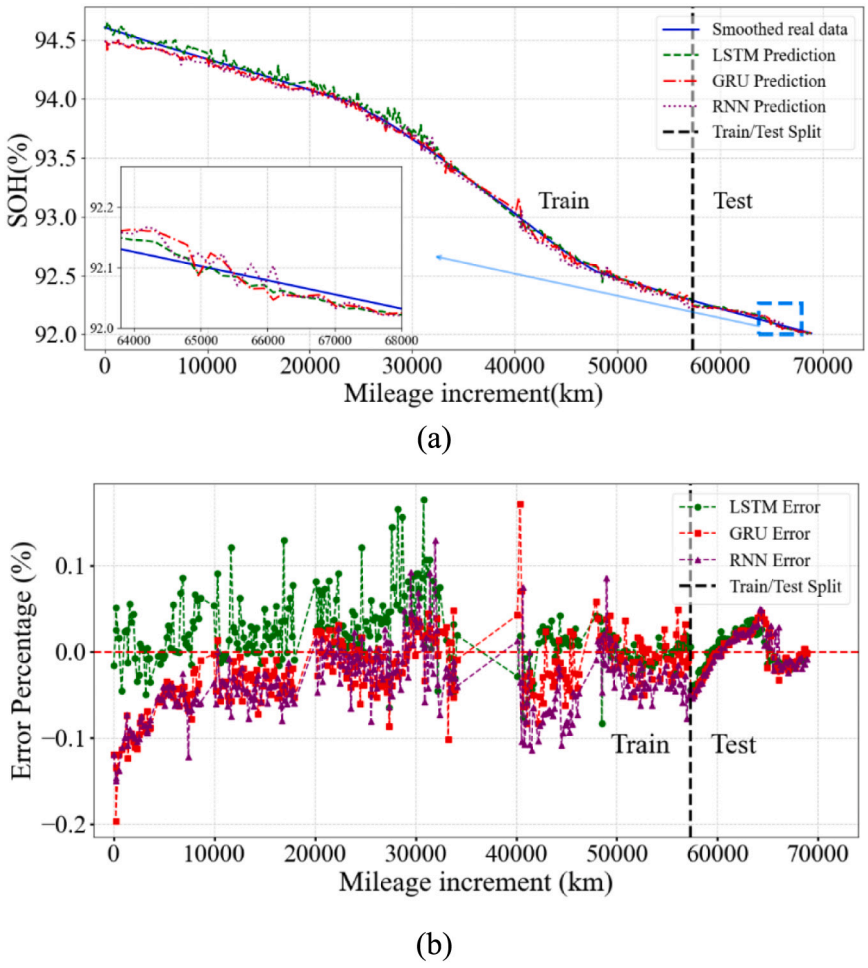

Fig. 8. SOH estimation results and errors at different algorithms. (a) SOH estimated results. (b) SOH estimated errors.

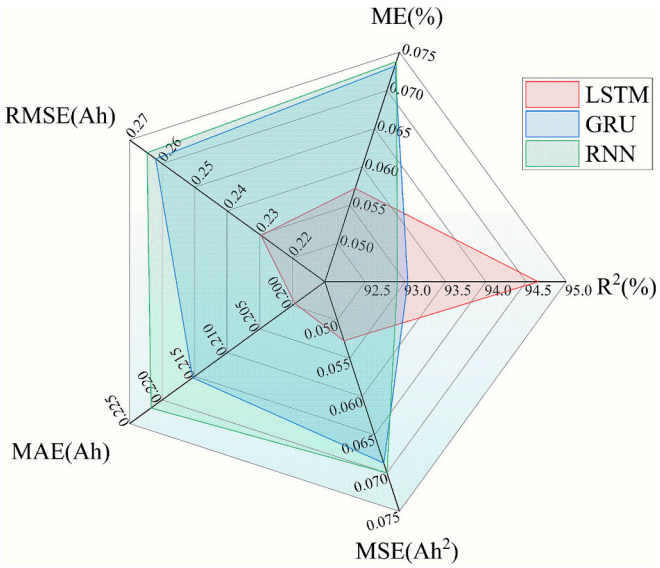

Fig. 9. SOH estimation metrics (ME, R^2, MSE, MAE, RMSE) results for different methods.

behaviors and diverse climatic conditions, demonstrating high reliability.

Fig. 13 further presents the error between the SOH values simulated by the EV-DOS model and the actual reference values. From the figure, it can be observed that the EV-DOS model not only effectively simulates the declining trend of battery SOH but also accurately captures the complex nonlinear characteristics of SOH variation. By capturing the evolution of battery performance during long-term operation, the model successfully represents the dynamic characteristics of battery performance degradation over the aging process. In terms of specific performance, the relative error between the simulated values and actual reference values of the EV-DOS model consistently remains within 0.6 %, indicating high accuracy and stability of the model's predictive capability under long-term operating conditions.

5. Evaluating driver behavior impacts on battery life with EV-DOS

The EV-DOS model leverages real-world vehicle data to establish an SOH model that effectively captures the impact of driving behaviors on battery aging, and it serves as a comprehensive framework capable of quantifying the effects of real-world driving and charging patterns over extended periods—spanning over a decade or more than 100,000 km. With this capability, the EV-DOS model enables the exploration of the long-term effects of various factors—charging depths, charging rates, HVAC usage, ambient temperature and V2G—on battery SOH across diverse geographic and operational contexts. These factors directly influence battery degradation through real-world usage patterns. Charging depths and rates capture drivers' charging habits, including preferences for fast charging or partial recharges, which affect thermal stress and cycling stability [12,61]. HVAC usage reflects energy

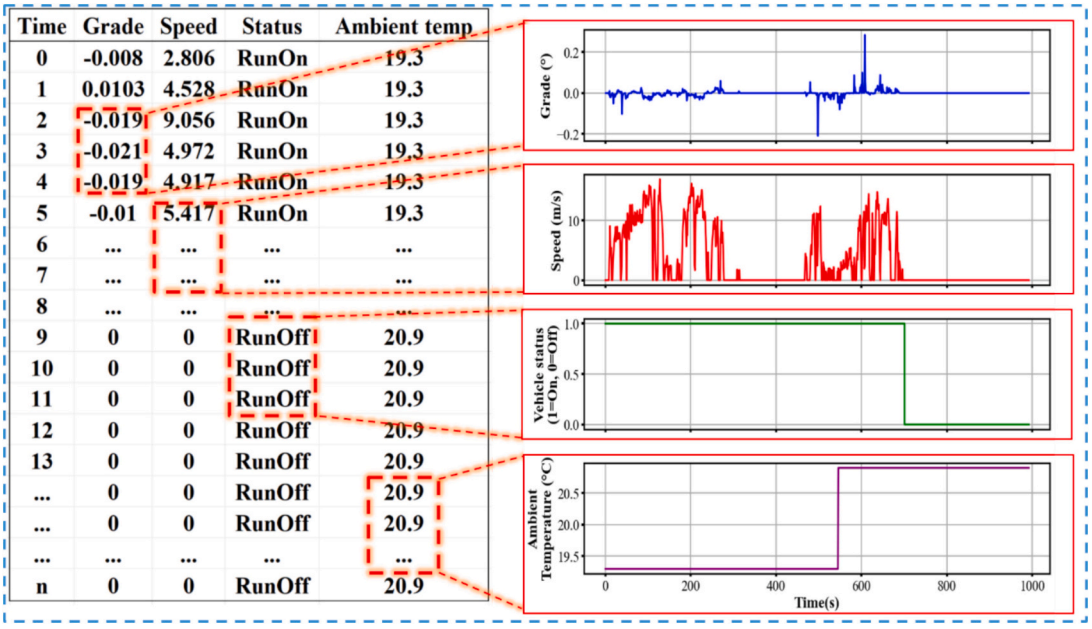

Fig. 10. Description of a single day's driving profile.

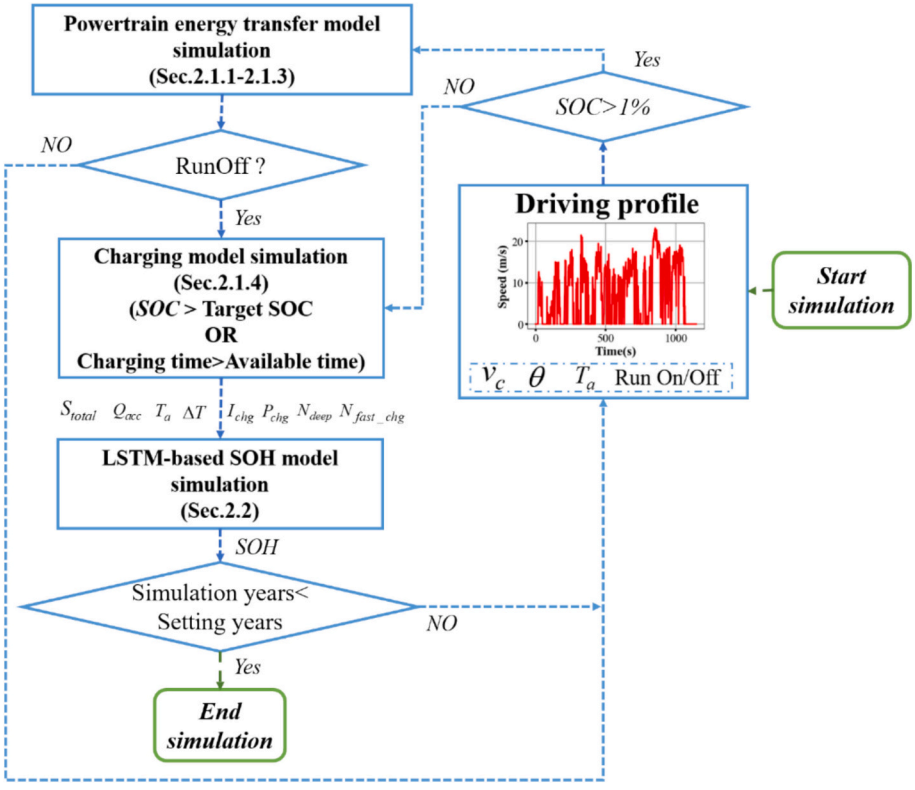

Fig. 11. Flow chart of the EV-DOS model for SOH.

consumption behaviors that vary with climate and personal preferences, impacting overall energy demand and battery wear [20]. Ambient temperature further contextualizes driving and charging conditions, as extreme climates amplify battery degradation [16,63]. V2G improves grid efficiency and offers economic benefits to drivers, but introduces additional charge-discharge cycles, which may accelerate battery degradation over time [21,51]. Together, these factors provide a comprehensive understanding of how everyday driver decisions shape long-term battery health.

The focus of this section is on private car usage. Compared to ride-hailing vehicles, private car users have a larger population base and stronger representativeness, which is of great significance for promoting and optimizing EVs among a broader user group. The driving profile adopted in Section 4.2 is based on ride-hailing vehicle users, with an average annual mileage of 70,000 to 100,000 km. In contrast, surveys indicate that the annual mileage of private cars typically ranges between 13,000 and 20,000 km [66,67]. To align with the typical usage patterns of private vehicles and minimize bias, this study proportionally scaled

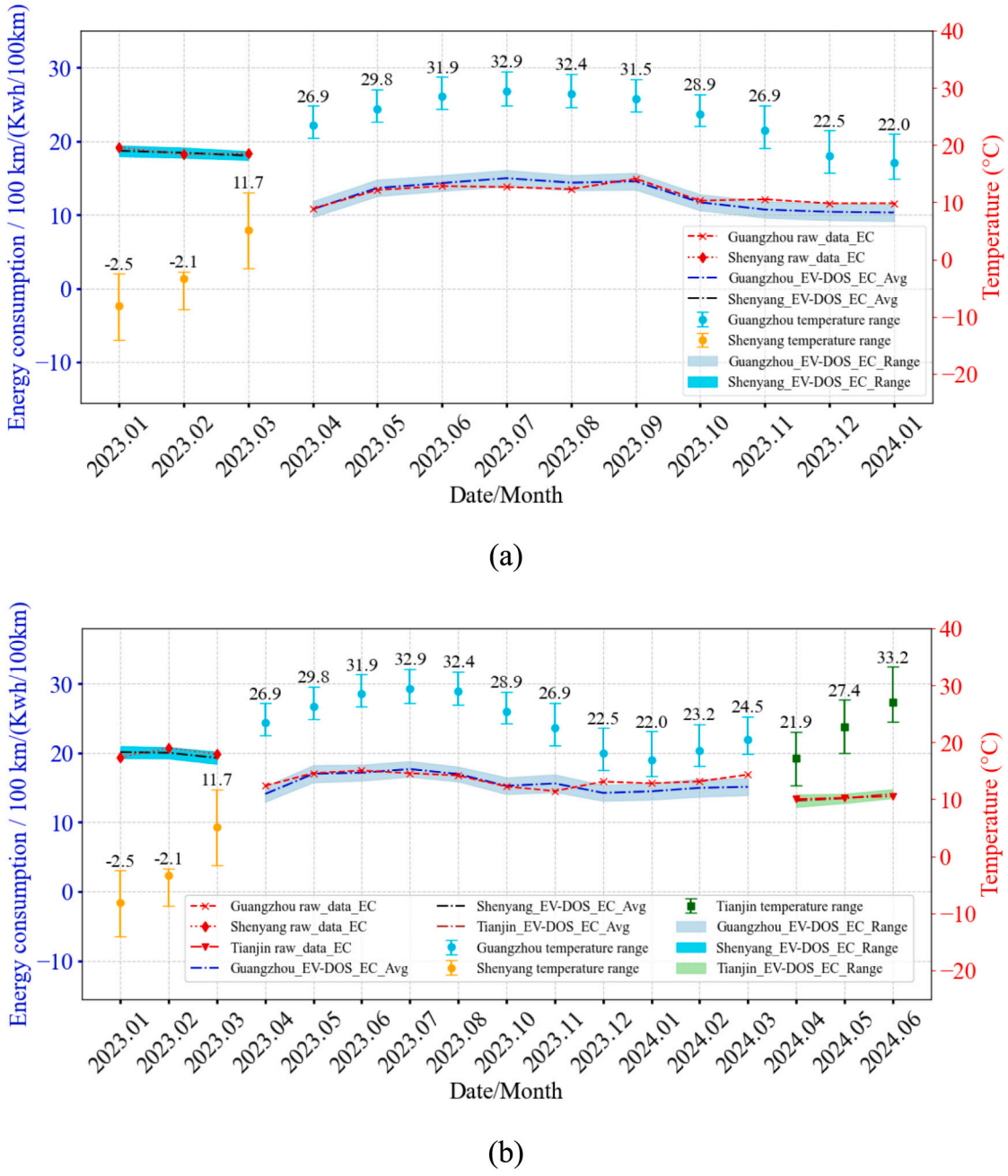

Fig. 12. EV-DOS model energy consumption verification. (a) Energy consumption comparison between Shenyang Vehicle No. 1 and Guangzhou Vehicle No. 1. (b) Energy consumption comparison between Shenyang Vehicle No. 2, Guangzhou Vehicle No. 2, and Tianjin No. 1.

down the monthly mileage of the driving profile established for a driver in Guangzhou in Section 3.1, limiting the total annual mileage to 20,000 km or less. In addition, to analyze the generalizability of the model across different geographical environments and driving behaviors, the study also incorporated the average driving characteristics of drivers in the New England region, derived from the publicly available National Household Travel Survey [55]. The main characteristic parameters of the two driving profiles from different regions used in this chapter are shown in Table 5.

5.1. *The impact of different charging depths on battery aging*

The study compares the degradation of battery SOH under two charging scenarios: charging to 80 % and charging to 95 % over a period of ten years, both utilizing Level 1 (L1) slow charging. Fig. 14 presents the degradation trends of battery SOH across different regions, drivers, and charging depths. The results show that, with increasing time and cumulative mileage, batteries exhibit varying degrees of degradation. However, deep charging, where batteries are charged to 95 %, results in significantly greater degradation. By the tenth year, under Guangzhou driving conditions, batteries charged to 95 % experienced an additional 3.12 % loss in SOH compared to those charged to 80 %. Under New England driving conditions, this gap increased to 4.22 %. Moreover, the changes in the box plot heights for the two charging depths reveal that deep charging significantly increases the variability of battery lifespan across different conditions. Further analysis reveals that, regardless of the region, the degradation curve for deep charging exhibits an accelerated downward trend, with the rate of degradation increasing gradually over time. In contrast, the degradation curve for charging to 80 % exhibits a more gradual decline.

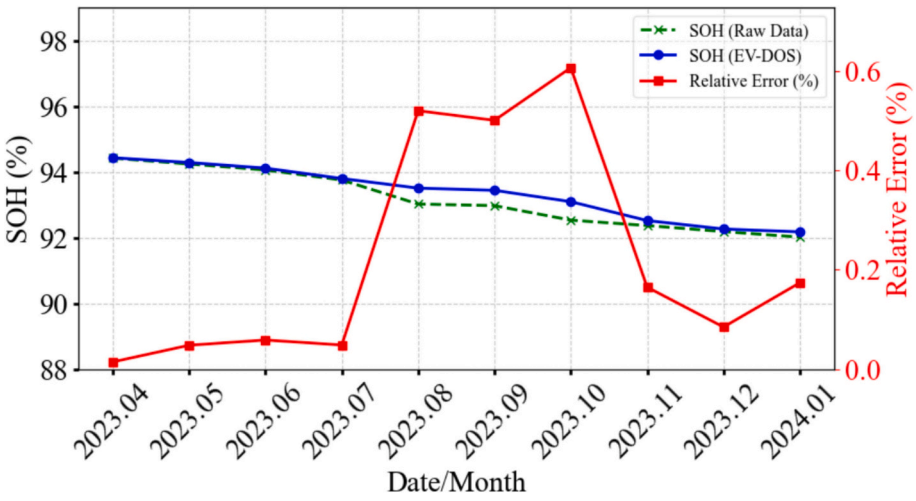

Fig. 13. EV-DOS model SOH result verification.

Table 5
The main characteristic parameters of the two driving conditions data.

Driving conditions	Total distance (km)	Average ambient temperature (°C)	Top speed (m/s)	Average speed (m/s)	Speed standard deviation (m/s)
Guangzhou	19,476	15–30	39.94	13.45	8.75
New England	19,597	−5–25	35.75	14.49	8.54

It is also notable that although the annual mileage in the Guangzhou and New England regions is similar, the New England region has lower ambient temperatures and higher average driving speeds. By the tenth year, under the charging to 80 % scenario, the SOH in Guangzhou is 0.06 % higher than in New England. However, under the charging to 95 % scenario, the SOH in Guangzhou is 1.16 % higher than in New England. This finding suggests that deep charging amplifies the impact of different driving conditions on battery SOH. In conclusion, reasonably controlling charging depth can significantly slow battery lifespan degradation, effectively reduce variability in battery lifespan, and partially mitigate the impact of different driving conditions on battery SOH. These findings provide valuable insights for optimizing charging strategies and extending the lifespan of EV batteries.

5.2. The impact of different charging rates on battery aging

This study also designed two additional control experiments, both targeting an 80 % charging level, using Level 1 slow charging and DC FC under the two driving conditions for a 10-year simulation to explore the effects of different charging rates on SOH. The key parameters of the two charging methods are shown in Table 6, and the simulation results are presented in Fig. 15. The results indicate that the DC FC significantly accelerates battery aging. By the tenth year, under Guangzhou driving conditions, batteries charged with DC FC experienced an additional 4.34 % SOH loss compared to those charged with L1 slow charging. In comparison, this gap widened to 5.08 % under New England driving conditions. Additionally, the changes in the height of the box plots indicate that DC FC results in greater variability in battery lifespan. However, unlike the degradation trend caused by deep charging, the degradation curve of DC FC shows a gradual flattening characteristic. As the simulation years increase, the rate of SOH decline decreases.

It is worth noting that under Guangzhou driving conditions, the battery lifespan degradation caused by DC fast charging was 0.8 % lower than under New England driving conditions. Overall, although fast charging significantly improves charging efficiency, it also accelerates the rate of battery degradation and increases variability. Furthermore, it amplifies the impact of different driving conditions on SOH.

Table 6
Types of chargers and their parameters.

Charger type	Charging power (kW)	Charging voltage (V)	Charging efficiency
Level 1	1.8	120	0.85
DC FC	60	480	0.85

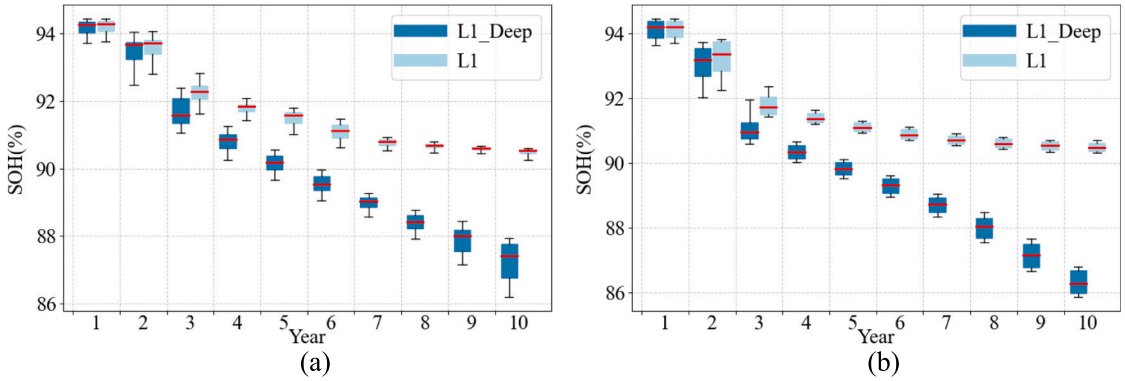

Fig. 14. Annual SOH degradation curve under different depths of charge. (a) Guangzhou simulation results. (b) New England simulation results.

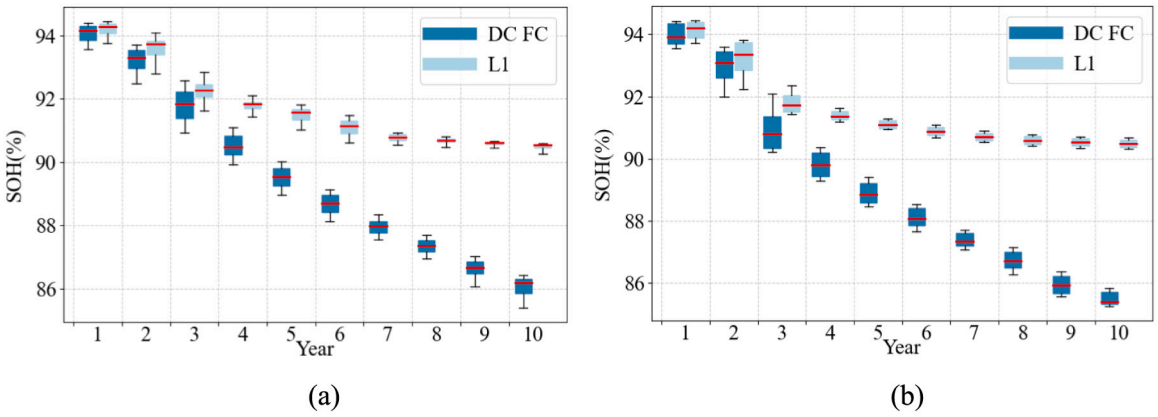

Fig. 15. Annual SOH degradation curve under different charging rates. (a) Guangzhou simulation results. (b) New England simulation results.

5.3. The impact of HVAC on SOH varies across different regions and driving conditions

This study investigates the impact of the HVAC system on battery SOH under driving conditions in Guangzhou and New England. Four comparative experiments were conducted: HVAC always on/off under Guangzhou driving conditions and HVAC always on/off under New England driving conditions. Fig. 16(a) displays the SOH degradation curves for the four experimental groups, all of which were driven under the same mileage. Fig. 16(b) presents the average monthly temperatures in Guangzhou and New England. As shown in Fig. 16(a), the HVAC system accelerates battery degradation regardless of the driving conditions or geographic location. Under the same mileage, the SOH under Guangzhou driving conditions is consistently higher than that under New England driving conditions. This is because the ambient temperature in Guangzhou falls within the optimal operating range for lithium-ion batteries. However, as mileage increases, the SOH difference between HVAC-on and HVAC-off scenarios widens under Guangzhou driving conditions, expanding to 0.5 % by the end of the simulation. In contrast, this difference remains relatively stable in New England.

To further explore the reasons behind the widening SOH difference under Guangzhou driving conditions, this study compared the average cabin temperatures and cumulative energy consumption of the HVAC system under HVAC-on scenarios in Guangzhou and New England over a

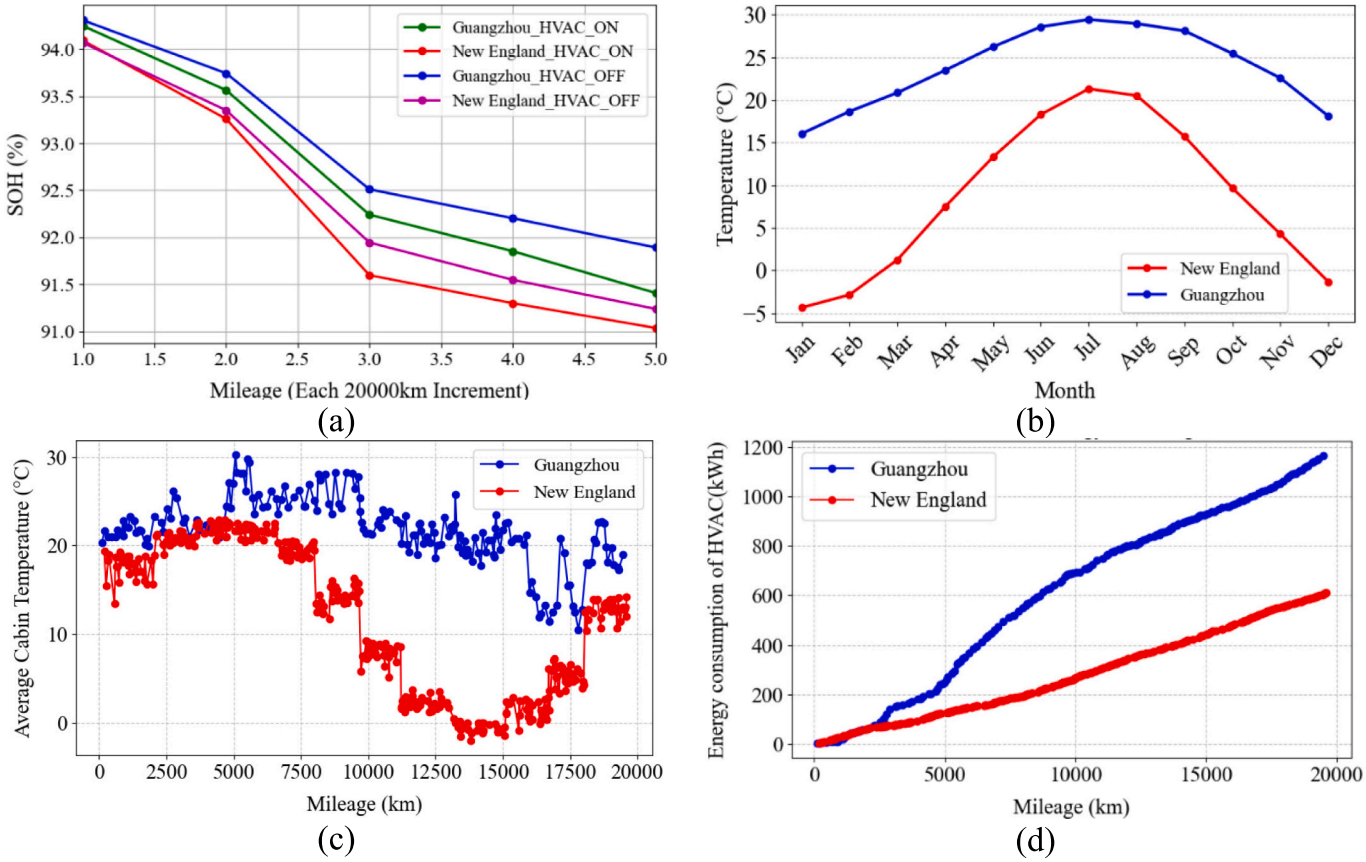

Fig. 16. The impact of HVAC and ambient temperature on battery SOH. (a) SOH comparison curves for Guangzhou and New England at the same mileage. (b) Monthly average ambient temperature in Guangzhou and New England. (c) Average cabin temperature in Guangzhou and New England over a year. (d) Comparison of cumulative energy consumption by HVAC system.

year. Fig. 16(c) shows that, due to the persistently high ambient temperatures in Guangzhou, the average cabin temperature is significantly higher than in New England. Fig. 16(d) reveals that, under the same mileage, the cumulative energy consumption of the HVAC system in Guangzhou is nearly 1.9 times higher than in New England. This is because, in Guangzhou, the HVAC system predominantly operates in cooling mode due to the high temperatures. According to Eq. (13) and Appendix Table A.1, the $COP_{cooling}$ is approximately 1/1.7 of that in heating mode, meaning that dissipating 1 kW of heat consumes about 1.7 times more energy than generating 1 kW of heat. The high energy consumption of the HVAC system under Guangzhou driving conditions effectively increases the battery's cycle count, directly accelerating battery degradation.

5.4. The impact of V2G across different regions and driving conditions

This study also examines the impact of V2G technology on battery lifespan over a long time period under two different driving scenarios. Specifically, the study adopts a "light V2G" scenario, where V2G activities only occur when the driver returns home at the end of each day [68]. In addition, the effects of different discharge depths are examined, specifically the cases of discharging to 10 % and 20 % under the V2G scenario. Fig. 17 and Table 7 illustrate the annual average SOH degradation curve under the V2G scenario for driving conditions in Guangzhou and New England. The results indicate that V2G behavior accelerates battery aging in both scenarios. After ten years of simulation, under the scenario of daily discharging to 20 %, the SOH degradation accelerates by more than 1.9 % compared to the case without V2G behavior. Furthermore, daily discharging to 10 % leads to an additional acceleration of battery aging by 0.9 %–1.4 % compared to daily discharging to 20 %. In conclusion, it is essential to control the depth of discharge for V2G reasonably. While considering the benefits of discharging, the impact of battery degradation should also be taken into account to achieve a balance between short-term gains and long-term benefits.

6. Conclusion

This study introduces the EV-DOS model, an innovative framework that integrates a physics-based powertrain energy transfer model with a data-driven SOH estimation module to quantify the long-term impacts of driving and charging behaviors on BEV battery health. While battery degradation has been well-characterized under controlled laboratory conditions, real-world variations in driving styles and charging behaviors introduce significant uncertainty, making accurate predictions challenging. The EV-DOS model addresses this complexity by incorporating real-world driving data and simulating battery performance across diverse geographic, ambient temperature, charging behavior, and operational contexts. Unlike conventional models that rely on simplified assumptions or focus on isolated factors, EV-DOS provides a comprehensive approach to evaluating how cumulative driving and charging behaviors influence long-term battery health.

The EV-DOS model is rigorously validated across different spatial and temporal scales, demonstrating high accuracy in simulating both energy consumption and battery degradation. The results show that the absolute monthly energy consumption error remains within 0.53 kWh/100 km, while the SOH estimation achieves a monthly average mistake of less than 0.6 %. Using the validated model, this study analyzes the effects of charging rate, charging depth, ambient temperature, HVAC usage, and V2G behavior under two distinct driving conditions. The findings reveal that DC FC significantly accelerates SOH degradation, with an observed increase of over 4 % in capacity loss over ten years compared to L1 charging. Similarly, deep charging to 95 % results in an additional 3 % degradation compared to maintaining an 80 % charge limit. Furthermore, V2G participation contributes to a further 1.9 % decline in SOH over a decade, with deeper discharge cycles amplifying the impact. Although higher ambient temperatures generally slow SOH degradation by keeping the battery within an optimal operating range, excessive HVAC usage under extreme conditions imposes additional energy demands, ultimately accelerating aging.

The EV-DOS model offers valuable insights into the interplay between driver behavior and battery longevity, providing researchers and industry stakeholders with a powerful tool to evaluate long-term battery performance. By identifying key operational factors that contribute to degradation, the model enables the development of targeted energy management strategies to optimize battery lifespan. However, certain limitations remain, presenting opportunities for future research:

1. Personalized Charging and V2G Optimization – Future studies could extend the EV-DOS model to develop personalized charging and V2G strategies tailored to driving patterns, optimizing battery lifespan, and economic value.

2. Integration with Energy Systems – The model could also integrate with campus-level energy systems, combining building energy, renewable generation, and storage models to create comprehensive energy management strategies.

These advancements will provide essential support for the smarter and more sustainable use of EV batteries, driving the development of next-generation energy solutions.

CRediT authorship contribution statement

Hao Jing: Writing – review & editing, Writing – original draft, Visualization, Validation, Software, Methodology, Formal analysis. **Jianyao Hu:** Data curation. **Shiqi (Shawn) Ou:** Writing – review & editing, Writing – original draft, Validation, Supervision, Project administration, Methodology, Investigation, Funding acquisition. **Xinwu Qian:** Writing – review & editing. **Hao Qi:** Writing – review & editing. **Jiankuan Zhu:** Writing – review & editing. **Haobo Dong:**

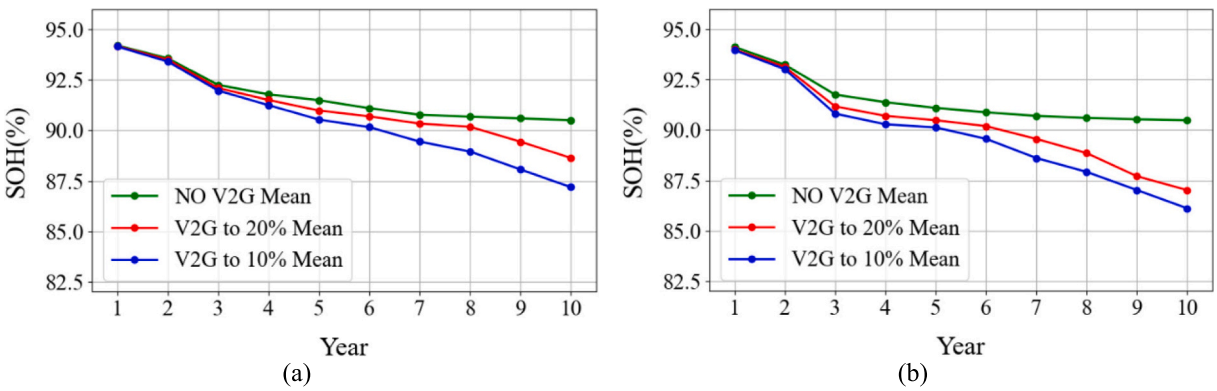

Fig. 17. Annual Average SOH Degradation Curve Under V2G. (a) Guangzhou simulation results. (b) New England simulation results.

Table 7
SOH change trend under different V2G scenarios.

Year	Scenario					
	Guangzhou NO V2G (%)	Guangzhou to 20 % (%)	Guangzhou to 10 % (%)	New England NO V2G (%)	New England to 20 % (%)	New England to 10 % (%)
1	94.21 ± 0.45	94.17 ± 0.50	94.16 ± 0.52	94.13 ± 0.42	94.00 ± 0.53	93.97 ± 0.57
2	93.58 ± 1.10	93.51 ± 0.80	93.42 ± 0.76	93.25 ± 1.01	93.14 ± 0.82	93.03 ± 1.27
3	92.25 ± 0.62	92.10 ± 0.70	91.97 ± 0.78	91.76 ± 0.59	91.18 ± 0.96	90.82 ± 0.71
4	91.79 ± 0.47	91.51 ± 0.76	91.25 ± 0.71	91.38 ± 0.24	90.71 ± 0.72	90.29 ± 0.97
5	91.50 ± 0.47	90.98 ± 0.68	90.53 ± 0.61	91.10 ± 0.19	90.49 ± 0.27	90.13 ± 1.21
6	91.10 ± 0.47	90.69 ± 0.49	90.16 ± 0.67	90.88 ± 0.21	90.20 ± 1.56	89.56 ± 0.55
7	90.77 ± 0.24	90.34 ± 0.24	89.45 ± 0.78	90.70 ± 0.19	89.56 ± 0.47	88.61 ± 1.10
8	90.68 ± 0.21	90.18 ± 0.53	88.95 ± 1.16	90.60 ± 0.19	88.86 ± 0.74	87.92 ± 0.63
9	90.59 ± 0.17	89.44 ± 1.52	88.06 ± 1.08	90.53 ± 0.20	87.71 ± 0.96	87.02 ± 0.69
10	90.50 ± 0.24	88.63 ± 2.18	87.19 ± 0.31	90.49 ± 0.20	87.02 ± 0.46	86.12 ± 0.58

Writing – review & editing.

Author statement

We declare that this manuscript is original, has not been published before and is not currently being considered for publication elsewhere.

We confirm that the manuscript has been read and approved by all named authors and that there are no other persons who satisfied the criteria for authorship but are not listed. We further confirm that the order of authors listed in the manuscript has been approved by all of us.

Declaration of competing interest

The authors declare that they have no known competing financial interests or personal relationships that could have appeared to influence the work reported in this paper.

Acknowledgment

This work is supported by the National Key Research and Development Program of China (2024YFE0115800) and the Introduced Innovative R&D Team of Guangdong Province (2023ZT10L145). All opinions expressed in this paper are the authors' and do not necessarily reflect the policies and views of sponsors.

Appendix A

Table A.1
Key parameters for vehicle powertrain system modeling.

Parameters	Descriptions	Value	Units
ρ_{air}	Air density	1.225	kg/m^3
A_d	Frontal area	2.13	m^2
c_d	Aerodynamic drag coefficient	0.35	–
c_r	Rolling resistance coefficient	0.015	–
g	Gravitational acceleration	9.81	m/s^2
σ	Rotational inertia correction factor	1.3	–
f_{rbs}	Brake energy recovery efficiency	0.63	–
K_{ab}	Heat transfer coefficient between environment and the battery	4.343	W/K
K_{bc}	Heat transfer coefficient between the battery and the cabin	3.468	W/K
C_{bat}	Battery pack heat capacity	101,771	J/K
C_{rated}	Default capacity of the battery	150	Ah
K_{btms}	Heat transfer coefficient between the battery and the battery management system	340	W/K
$T_{b,up}$	Maximum battery temperature setting	30	$^\circ C$
$T_{b,\mathrm{low}}$	Minimum battery temperature setting	10	$^\circ C$
K_{ac}	Heat transfer coefficient between environment and the cabin	22.6	W/K
K_{bc}	Heat transfer coefficient between the battery and the cabin	3.468	W/K
C_c	Cabin heat capacity	182,000	J/K
C_{HVAC}	HVAC constant	500.4	–
$COP_{cooling}$	The ratio of heat dissipation when HVAC works for cooling	1.5	–
$COP_{heating}$	The ratio of electrical power intake when HVAC works for heating	2.5	–

Data availability

Data will be made available on request.

References

[1] S. Hong, C. Qin, X. Lai, et al., State-of-health estimation and remaining useful life prediction for lithium-ion batteries based on an improved particle filter algorithm, J. Energy Storage 64 (2023) 107179, https://doi.org/10.1016/j.est.2023.107179.

[2] Y. Zheng, Y. Cui, X. Han, et al., Lithium-ion battery capacity estimation based on open circuit voltage identification using the iteratively reweighted least squares at different aging levels, J. Energy Storage 44 (2021) 103487, https://doi.org/10.1016/j.est.2021.103487.
[3] X. Xiong, Y. Wang, C. Jiang, et al., End-to-end deep learning powered battery state of health estimation considering multi-neighboring incomplete charging data, Energy 292 (2024) 130495, https://doi.org/10.1016/j.energy.2024.130495.
[4] International Energy Agency, Global EV Outlook 2024, 2024. Available at: https://www.iea.org/reports/global-ev-outlook-2024. (Accessed 28 November 2024).
[5] X. Yu, T. Tang, Z. Song, et al., State-of-health estimation for lithium-ion batteries under complex charging conditions based on SDE-BiLSTM model, J. Energy Storage 111 (2025) 115352, https://doi.org/10.1016/j.est.2025.115352.
[6] X. Wu, Z. Zuo, P. Liu, User behavior optimization strategy for electric vehicle based on improving battery SOH[C], in: Proceedings of China SAE Congress 2021: Selected Papers, Springer Nature Singapore, Singapore, 2022, pp. 1223–1236, https://doi.org/10.1007/978-981-19-3842-9_95.
[7] Y. Lu, J. Lin, D. Guo, et al., Towards real-world state of health estimation, part 1: cell-level method using lithium-ion battery laboratory data, eTransportation 21 (2024) 100338, https://doi.org/10.1016/j.etran.2024.100338.
[8] N. Jiang, J. Zhang, W. Jiang, et al., Driving behavior-guided battery health monitoring for electric vehicles using extreme learning machine, Appl. Energy 364 (2024) 123122, https://doi.org/10.1016/j.apenergy.2024.123122.
[9] S. Onori, P. Spagnol, V. Marano, et al., A new life estimation method for lithium-ion batteries in plug-in hybrid electric vehicles applications, Int. J. Power Electron. 4 (3) (2012) 302–319, https://doi.org/10.1504/IJPELEC.2012.046609.
[10] Z. Xu, X. Yan, B. Huang, et al., The effect of charge behavior on lithium battery SOH[C], in: 2020 3rd International Conference on Advanced Electronic Materials, Computers and Software Engineering (AEMCSE), IEEE, 2020, pp. 658–661, https://doi.org/10.1109/AEMCSE50948.2020.00144.
[11] M. Shirk, J. Wishart, Effects of Electric Vehicle Fast Charging on Battery Life and Vehicle Performance [R], Idaho National Lab. (INL), Idaho Falls, ID (United States), 2015.
[12] S.J. Park, Y.W. Song, B.S. Kang, et al., Depth of discharge characteristics and control strategy to optimize electric vehicle battery life, J. Energy Storage 59 (2023) 106477, https://doi.org/10.1016/j.est.2022.106477.
[13] E. Wikner, T. Thiringer, Extending battery lifetime by avoiding high SOC, Appl. Sci. 8 (10) (2018) 1825, https://doi.org/10.3390/app8101825.
[14] R. Gauthier, A. Luscombe, T. Bond, et al., How do depth of discharge, C-rate and calendar age affect capacity retention, impedance growth, the electrodes, and the electrolyte in Li-ion cells? J. Electrochem. Soc. 169 (2) (2022) 020518 https://doi.org/10.1149/1945-7111/ac4b82.
[15] S. Sun, T. Guan, B. Shen, et al., Changes of degradation mechanisms of LiFePO4/graphite batteries cycled at different ambient temperatures, Electrochim. Acta 237 (2017) 248–258, https://doi.org/10.1016/j.electacta.2017.03.158.
[16] A.B. Nemati, S.M. Mousavi-Khoshdel, G.R. Molaeimanesh, et al., Effects of ambient temperature on the health characteristics of vehicular Li-ion batteries by electrochemical impedance spectroscopy, J. Therm. Anal. Calorim. 146 (2021) 665–672, https://doi.org/10.1007/s10973-020-10052-y.
[17] W. Zhang, Q. Sun, X. Zhou, et al., Investigation on the thermal behavior of thermal management system for battery pack with heat pipe based on multiphysics coupling model, Energy 308 (2024) 133053, https://doi.org/10.1016/j.energy.2024.133053.
[18] Q. Tang, Y. Yang, C. Luo, et al., A novel electro-hydraulic compound braking system coordinated control strategy for a four-wheel-drive pure electric vehicle driven by dual motors, Energy 241 (2022) 122750, https://doi.org/10.1016/j.energy.2021.122750.
[19] R.K. Chidambaram, D. Chatterjee, B. Barman, et al., Effect of regenerative braking on battery life, Energies 16 (14) (2023) 5303, https://doi.org/10.3390/en16145303.
[20] K. Vatanparvar, M.A. Al Faruque, Battery lifetime-aware automotive climate control for electric vehicles [C], in: Proceedings of the 52nd Annual Design Automation Conference, 2015, pp. 1–6, https://doi.org/10.1145/2744769.2744804.
[21] S. Sagaria, M. van der Kam, T. Boström, Vehicle-to-grid impact on battery degradation and estimation of V2G economic compensation, Appl. Energy 377 (2025) 124546, https://doi.org/10.1016/j.apenergy.2024.124546.
[22] P. Huang, P. Gu, Y. Kang, et al., The state of health estimation of lithium-ion batteries based on data-driven and model fusion method, J. Clean. Prod. 366 (2022) 132742, https://doi.org/10.1016/j.jclepro.2022.132742.
[23] Z. Deng, X. Lin, J. Cai, et al., Battery health estimation with degradation pattern recognition and transfer learning, J. Power Sources 525 (2022) 231027, https://doi.org/10.1016/j.jpowsour.2022.231027.
[24] K.S. Ng, C.S. Moo, Y.P. Chen, et al., Enhanced coulomb counting method for estimating state-of-charge and state-of-health of lithium-ion batteries, Appl. Energy 86 (9) (2009) 1506–1511, https://doi.org/10.1016/j.apenergy.2008.11.021.
[25] Z. Guo, X. Qiu, G. Hou, et al., State of health estimation for lithium ion batteries based on charging curves, J. Power Sources 249 (2014) 457–462, https://doi.org/10.1016/j.jpowsour.2013.10.114.
[26] M. Galeotti, L. Cinà, C. Giammanco, et al., Performance analysis and SOH (state of health) evaluation of lithium polymer batteries through electrochemical impedance spectroscopy, Energy 89 (2015) 678–686, https://doi.org/10.1016/j.energy.2015.05.148.
[27] H. Ren, Y. Zhao, S. Chen, et al., Design and implementation of a battery management system with active charge balance based on the SOC and SOH online estimation, Energy 166 (2019) 908–917, https://doi.org/10.1016/j.energy.2018.10.133.
[28] S. Wang, P. Takyi-Aninakwa, Y. Fan, et al., A novel feedback correction-adaptive Kalman filtering method for the whole-life-cycle state of charge and closed-circuit voltage prediction of lithium-ion batteries based on the second-order electrical equivalent circuit model, Int. J. Electr. Power Energy Syst. 139 (2022) 108020, https://doi.org/10.1016/j.ijepes.2022.108020.
[29] J. Tian, R. Xiong, Q. Yu, Fractional-order model-based incremental capacity analysis for degradation state recognition of lithium-ion batteries, IEEE Trans. Ind. Electron. 66 (2) (2018) 1576–1584, https://doi.org/10.1109/TIE.2018.2798606.
[30] G.K. Prasad, C.D. Rahn, Model based identification of aging parameters in lithium ion batteries, J. Power Sources 232 (2013) 79–85, https://doi.org/10.1016/j.jpowsour.2013.01.041.
[31] J. Li, K. Adewuyi, N. Lotfi, et al., A single particle model with chemical/mechanical degradation physics for lithium ion battery State of Health (SOH) estimation, Appl. Energy 212 (2018) 1178–1190, https://doi.org/10.1016/j.apenergy.2018.01.011.
[32] E. Kheirkhah-Rad, M. Moeini-Aghtaie, A novel data-driven SOH prediction model for lithium-ion batteries[C], in: 2021 31st Australasian Universities Power Engineering Conference (AUPEC), IEEE, 2021, pp. 1–6, https://doi.org/10.1109/AUPEC52110.2021.9597754.
[33] J. Hong, K. Li, F. Liang, et al., A novel state of health prediction method for battery system in real-world vehicles based on gated recurrent unit neural networks, Energy 289 (2024) 129918, https://doi.org/10.1016/j.energy.2023.129918.
[34] X. Zhao, J. Hu, G. Hu, et al., A state of health estimation framework based on real-world electric vehicles operating data, J. Energy Storage 63 (2023) 107031, https://doi.org/10.1016/j.est.2023.107031.
[35] H. Xu, L. Wu, S. Xiong, et al., An improved CNN-LSTM model-based state-of-health estimation approach for lithium-ion batteries, Energy 276 (2023) 127585, https://doi.org/10.1016/j.energy.2023.127585.
[36] C. Zhang, L. Luo, Z. Yang, et al., Battery SOH estimation method based on gradual decreasing current, double correlation analysis and GRU, Green Energy Intell. Transp 2 (5) (2023) 100108, https://doi.org/10.1016/j.geits.2023.100108.
[37] C. Zhang, Y. Zhou, Z. Zhou, et al., State of health estimation of lithium-ion batteries based on multiphysics features and CNN-EFC-BiLSTM, IEEE Sensors J. (2024), https://doi.org/10.1109/JSEN.2024.3476188.
[38] M. Berecibar, I. Gandiaga, I. Villarreal, et al., Critical review of state of health estimation methods of Li-ion batteries for real applications, Renew. Sust. Energ. Rev. 56 (2016) 572–587, https://doi.org/10.1016/j.rser.2015.11.042.
[39] L. Vichard, A. Ravey, P. Venet, et al., A method to estimate battery SOH indicators based on vehicle operating data only, Energy 225 (2021) 120235, https://doi.org/10.1016/j.energy.2021.120235.
[40] S.B. Vilsen, D.I. Stroe, Battery state-of-health modelling by multiple linear regression, J. Clean. Prod. 290 (2021) 125700, https://doi.org/10.1016/j.jclepro.2020.125700.
[41] M. Dong, X. Li, Z. Yang, et al., State of health (SOH) assessment for LIBs based on characteristic electrochemical impedance, J. Power Sources 603 (2024) 234386, https://doi.org/10.1016/j.jpowsour.2024.234386.
[42] J. Hong, F. Liang, H. Yang, et al., Multi-forword-step state of charge prediction for real-world electric vehicles battery systems using a novel LSTM-GRU hybrid neural network, eTransportation 20 (2024) 100322, https://doi.org/10.1016/j.etran.2024.100322.
[43] F. Wang, Z. Zhai, Z. Zhao, et al., Physics-informed neural network for lithium-ion battery degradation stable modeling and prognosis, Nat. Commun. 15 (1) (2024) 4332, https://doi.org/10.1038/s41467-024-48779-z.
[44] L. Chen, S. Xie, A.M. Lopes, et al., A new SOH estimation method for Lithium-ion batteries based on model-data-fusion, Energy 286 (2024) 129597, https://doi.org/10.1016/j.energy.2023.129597.
[45] C. Zhang, L. Tu, Z. Yang, et al., A CMMOG-based lithium-battery SOH estimation method using multi-task learning framework, J. Energy Storage 107 (2025) 114884, https://doi.org/10.1016/j.est.2024.114884.
[46] X. Bao, L. Chen, A.M. Lopes, et al., Hybrid deep neural network with dimension attention for state-of-health estimation of lithium-ion batteries, Energy 278 (2023) 127734, https://doi.org/10.1016/j.energy.2023.127734.
[47] C. Zhang, L. Luo, Z. Yang, et al., Flexible method for estimating the state of health of lithium-ion batteries using partial charging segments, Energy 295 (2024) 131009, https://doi.org/10.1016/j.energy.2024.131009.
[48] G. Pozzato, A. Allam, L. Pulvirenti, et al., Analysis and key findings from real-world electric vehicle field data, Joule 7 (9) (2023) 2035–2053, https://doi.org/10.1016/j.joule.2023.07.018.
[49] A. Cordoba-Arenas, S. Onori, G. Rizzoni, A control-oriented lithium-ion battery pack model for plug-in hybrid electric vehicle cycle-life studies and system design with consideration of health management, J. Power Sources 279 (2015) 791–808, https://doi.org/10.1016/j.jpowsour.2014.12.048.
[50] Y.Y. Soo, Y. Wang, H. Xiang, et al., Machine learning based battery pack health prediction using real-world data, Energy 308 (2024) 132856, https://doi.org/10.1016/j.energy.2024.132856.
[51] D. Wang, J. Coignard, T. Zeng, et al., Quantifying electric vehicle battery degradation from driving vs. vehicle-to-grid services, J. Power Sources 332 (2016) 193–203, https://doi.org/10.1016/j.jpowsour.2016.09.116.
[52] S. Bashash, S.J. Moura, J.C. Forman, et al., Plug-in hybrid electric vehicle charge pattern optimization for energy cost and battery longevity, J. Power Sources 196 (1) (2011) 541–549, https://doi.org/10.1016/j.jpowsour.2010.07.001.
[53] A. Millner, Modeling lithium ion battery degradation in electric vehicles[C], in: 2010 IEEE Conference on Innovative Technologies for an Efficient and Reliable Electricity Supply, IEEE, 2010, pp. 349–356, https://doi.org/10.1109/CITRES.2010.5619782.
[54] S. Grolleau, A. Delaille, H. Gualous, et al., Calendar aging of commercial graphite/LiFePO4 cell–predicting capacity fade under time dependent storage conditions,

J. Power Sources 255 (2014) 450–458, https://doi.org/10.1016/j.jpowsour.2013.11.098.
[55] S. Ou, Estimate long-term impact on battery degradation by considering electric vehicle real-world end-use factors, J. Power Sources 573 (2023) 233133, https://doi.org/10.1016/j.jpowsour.2023.233133.
[56] M. Jiao, D. Wang, J. Qiu, A GRU-RNN based momentum optimized algorithm for SOC estimation, J. Power Sources 459 (2020) 228051, https://doi.org/10.1016/j.jpowsour.2020.228051.
[57] S. Khaleghi, Y. Firouz, J. Van Mierlo, et al., Developing a real-time data-driven battery health diagnosis method, using time and frequency domain condition indicators, Appl. Energy 255 (2019) 113813, https://doi.org/10.1016/j.apenergy.2019.113813.
[58] Visual Crossing Weather, Historical weather data API. https://www.visualcrossing.com/weather-data;, 2024. (Accessed 22 December 2024).
[59] D. Kim, G. Seomun, Y. Lee, et al., Forecasting building energy demand and on-site power generation for residential buildings using long and short-term memory method with transfer learning, Appl. Energy 368 (2024) 123500, https://doi.org/10.1016/j.apenergy.2024.123500.
[60] Open Topo Data, High-resolution elevation data API. https://www.opentopodata.org/;, 2024. (Accessed 22 December 2024).
[61] Z. He, X. Shen, Y. Sun, et al., State-of-health estimation based on real data of electric vehicles concerning user behavior, J. Energy Storage 41 (2021) 102867, https://doi.org/10.1016/j.est.2021.102867.
[62] D. Zhang, Z. Wang, P. Liu, et al., Multistep fast charging-based state of health estimation of lithium-ion batteries, IEEE Trans. Transp. Electrif. 10 (3) (2023) 4640–4652, https://doi.org/10.1109/TTE.2023.3322582.
[63] Z. Gao, H. Xie, X. Yang, et al., SOH estimation method for lithium-ion batteries under low temperature conditions with nonlinear correction, J. Energy Storage 75 (2024) 109690, https://doi.org/10.1016/j.est.2023.109690.
[64] S. Wen, N. Lin, S. Huang, et al., Lithium battery state of health estimation using real-world vehicle data and an interpretable hybrid framework, J. Energy Storage 96 (2024) 112623, https://doi.org/10.1016/j.est.2024.112623.
[65] F. Xia, Y. Yu, J. Chen, SOH and RUL prediction of lithium batteries based on fusions of RLOESS filtered electrochemical and thermal features by bidirectional gated recurrent unit network, J. Energy Storage 102 (2024) 114134, https://doi.org/10.1016/j.est.2024.114134.
[66] Fleet News Daily, Average Age of Vehicles in the US Increases to 12.2 Years According to SP Global Mobility, 2022. Available at: https://fleetnewsdaily.com/average-age-of-vehicles-in-the-us-increases-to-12-2-years-according-to-sp-global-mobility. (Accessed 30 November 2024).
[67] IHS Markit, Vehicle miles traveled in the U.S, Available at: https://cdn.ihsmarkit.com/www/pdf/0122/Vehicle-Miles-Traveled.pdf, 2021. (Accessed 30 November 2024).
[68] M. Petit, E. Prada, V. Sauvant-Moynot, Development of an empirical aging model for Li-ion batteries and application to assess the impact of Vehicle-to-Grid strategies on battery lifetime, Appl. Energy 172 (2016) 398–407, https://doi.org/10.1016/j.apenergy.2016.03.119.